

## Asymptotic normalization coefficients for $\alpha + {}^{12}\text{C}$ synthesis and the $S$ factor for ${}^{12}\text{C}(\alpha, \gamma){}^{16}\text{O}$ radiative capture

A. M. Mukhamedzhanov <sup>1,\*</sup>, R. J. deBoer <sup>2</sup>, B. F. Irgaziev <sup>3</sup>, L. D. Blokhintsev,<sup>4</sup> A. S. Kadyrov <sup>5,6</sup> and D. A. Savin <sup>4</sup>

<sup>1</sup>*Cyclotron Institute, Texas A&M University, College Station, Texas 77843, USA*

<sup>2</sup>*Department of Physics and Astronomy and the Joint Institute for Nuclear Astrophysics, University of Notre Dame, Notre Dame, Indiana 46556, USA*

<sup>3</sup>*Theoretical Physics Department, National University of Uzbekistan, Tashkent 100174, Uzbekistan*

<sup>4</sup>*Skobeltsyn Institute of Nuclear Physics, Lomonosov Moscow State University, Moscow 119991, Russia*

<sup>5</sup>*Department of Physics and Astronomy, Curtin University, GPO Box U1987, Perth, WA 6845, Australia*

<sup>6</sup>*Institute of Nuclear Physics, Ulugbek, Tashkent 100214, Uzbekistan*



(Received 9 March 2024; revised 2 July 2024; accepted 22 October 2024; published 19 November 2024)

**Background:** The  ${}^{12}\text{C}(\alpha, \gamma){}^{16}\text{O}$  reaction, determining the survival of carbon in red giants, is of interest for nuclear reaction theory and nuclear astrophysics. A specific feature of the  ${}^{16}\text{O}$  nuclear structure is the presence of two subthreshold bound states, (6.92 MeV,  $2^+$ ) and (7.12 MeV,  $1^-$ ), that dominate the behavior of the low-energy  $S$  factor. The strength of these subthreshold states is determined by their asymptotic normalization coefficients (ANCs), which need to be known with high accuracy.

**Purpose:** The objective of this research is to examine how the subthreshold and ground-state ANCs impact the low-energy  $S$  factor, especially at the key astrophysical energy of 300 keV.

**Method:** The  $S$  factors are calculated within the framework of the  $R$ -matrix method using the AZURE2 code.

**Results:** Our total  $S$  factor takes into account the  $E1$  and  $E2$  transitions to the ground state of  ${}^{16}\text{O}$  including the interference of the subthreshold and higher resonances, which also interfere with the corresponding direct captures, and cascade radiative captures to the ground state of  ${}^{16}\text{O}$  through four subthreshold states:  $0_2^+$ ,  $3^-$ ,  $2^+$ , and  $1^-$ . To evaluate the impact of subthreshold ANCs on the low-energy  $S$  factor, we employ two sets of the ANCs. The first selection, which offers higher ANC values, is attained through the extrapolation process [Blokhintsev *et al.*, *Eur. Phys. J. A* **59**, 162 (2023)]. The set with low ANC values was employed by deBoer *et al.* [*Rev. Mod. Phys.* **89**, 035007 (2017)]. A detailed comparison of the  $S$  factors at the most effective astrophysical energy of 300 keV is provided, along with an investigation into how the ground-state ANC affects this  $S$  factor.

**Conclusion:** The contribution to the total  $E1$  and  $E2$   $S$  factors from the corresponding subthreshold resonances at 300 keV are (71–74)% and (102–103)%, respectively. The correlation of the uncertainties of the subthreshold ANCs with the  $E1$  and  $E2$   $S(300\text{ keV})$  factors is found. The  $E1$  transition of the subthreshold resonance  $1^-$  does not depend on the ground-state ANC but interferes constructively with a broad (9.585 MeV;  $1^-$ ) resonance giving (for the present subthreshold ANC) an additional 26% contribution to the total  $E1$   $S(300\text{ keV})$  factor. Interference of the  $E2$  transition through the subthreshold resonance  $2^+$  with direct capture is almost negligible for small ground-state ANC of  $58\text{ fm}^{-1/2}$ . However, its interference with direct capture for higher ground-state ANC of  $337\text{ fm}^{-1/2}$  is significant and destructive, contributing  $-27\%$ . The low-energy  $S_{E2}(300\text{ keV})$  factor experiences a smaller increase when both subthreshold and the ground-state ANCs rise together due to their anticorrelation, compared to when only the subthreshold ANCs increase.

DOI: [10.1103/PhysRevC.110.055803](https://doi.org/10.1103/PhysRevC.110.055803)

### I. INTRODUCTION

The  ${}^{12}\text{C}/{}^{16}\text{O}$  ratio in red giant stars has been attracting substantial scientific attention for a long time [1,2]. While

${}^{12}\text{C}$  is formed via the triple- $\alpha$  fusion,  ${}^{16}\text{O}$  is the result of the  ${}^{12}\text{C}(\alpha, \gamma){}^{16}\text{O}$  radiative capture reaction, which determines the survival of carbon. Numerous attempts to obtain the astrophysical factor of the  ${}^{12}\text{C}(\alpha, \gamma){}^{16}\text{O}$  reaction, both experimental and theoretical, have been made for almost 50 years (see Refs. [1–18] and references therein). The latest comprehensive and thorough review of the state of the art has been presented in Ref. [2].

The main goal of the research is to obtain the astrophysical  $S$  factor for the  ${}^{12}\text{C}(\alpha, \gamma){}^{16}\text{O}$  radiative capture in the Gamow window with the most effective astrophysical  $\alpha$ - ${}^{12}\text{C}$  relative kinetic energy  $E = 300\text{ keV}$  with the accuracy  $<10\%$ .

\* Contact author: akram@comp.tamu.edu

Published by the American Physical Society under the terms of the [Creative Commons Attribution 4.0 International](https://creativecommons.org/licenses/by/4.0/) license. Further distribution of this work must maintain attribution to the author(s) and the published article's title, journal citation, and DOI.

TABLE I. ANC  $C_l$  values in  $\text{fm}^{-1/2}$  for  $^{16}\text{O}^*(J^\pi) \rightarrow \alpha + ^{12}\text{C}$  (g.s.).

$C_0; J^\pi = 0^+$ $\varepsilon = 1.113 \text{ MeV}$	$C_3; J^\pi = 3^-$ $\varepsilon = 1.032 \text{ MeV}$	$C_2; J^\pi = 2^+$ $\varepsilon = 0.245 \text{ MeV}$	$C_1; J^\pi = 1^-$ $\varepsilon = 0.045 \text{ MeV}$	References
		$(1.11 \pm 0.10) \times 10^5$	$(2.08 \pm 0.19) \times 10^{14}$	[9]
		$(1.40 \pm 0.42) \times 10^5$	$(1.87 \pm 0.32) \times 10^{14}$	[12]
		$(1.44 \pm 0.26) \times 10^5$	$(2.00 \pm 0.69) \times 10^{14}$	[27]
$(1.56 \pm 0.09) \times 10^3$	$(1.39 \pm 0.08) \times 10^2$	$(1.22 \pm 0.06) \times 10^5$	$(2.10 \pm 0.14) \times 10^{14}$	[17]
		$0.213 \times 10^5$	$1.03 \times 10^{14}$	[28]
$0.4057 \times 10^3$		$0.505 \times 10^5$	$2.073 \times 10^{14}$	[29]
		$(1.10-1.31) \times 10^5$	$2.21(0.07) \times 10^{14}$	[30]
$(0.64-0.74) \times 10^3$	$(1.2-1.5) \times 10^2$	$(0.21-0.24) \times 10^5$	$(1.6-1.9) \times 10^{14}$	[31]
$0.293 \times 10^3$				[32]
$1.34 \times 10^3$	$1.22 \times 10^2$	$(0.98-1.07) \times 10^5$	$(1.83-1.84) \times 10^{14}$	[33]
$1.56 \times 10^3$	$1.39 \times 10^2$	$1.14 \times 10^5$	$2.08 \times 10^{14}$	[2]
$(0.886-1.139) \times 10^3$				[21]
	$(2.17 \pm 0.05) \times 10^2$	$(1.42 \pm 0.05) \times 10^5$	$(2.27 \pm 0.02) \times 10^{14}$	[22]

However, this goal is far from being achieved because at this energy direct measurements are hardly feasible due to the extremely small cross section.<sup>1</sup> Extrapolating down the experimental data available at energies  $E > 1 \text{ MeV}$  to the low-energy region allows one to obtain the  $S(300 \text{ keV})$  factor. The most popular method of the extrapolation is the  $R$ -matrix approach [2]. It provides a way to control contributions of different interfering mechanisms of the radiative capture and impact of different input parameters.

It is very well known (see, for example, Refs. [2,9] and references therein) that one of the important parameters for extrapolation of the experimental data to the low-energy region and determination of the  $S(300 \text{ keV})$  factor are the asymptotic normalization coefficients (ANCs) for the  $\alpha + ^{12}\text{C} \rightarrow ^{16}\text{O}(7.12 \text{ MeV}, 1^-)$  and  $\alpha + ^{12}\text{C} \rightarrow ^{16}\text{O}(6.92 \text{ MeV}, 2^+)$  syntheses leading to the formation of two subthreshold (that is, near the  $\alpha + ^{12}\text{C}$  threshold) bound states,  $1^-$  and  $2^+$ . The binding energies of these bound states are  $\varepsilon_{s1} = 0.045 \text{ MeV}$  and  $\varepsilon_{s2} = 0.2449 \text{ MeV}$ , respectively. Since these subthreshold states are the closest levels to the low-energy region  $E < 0.5 \text{ MeV}$  (the nearest  $1^-$  and  $2^+$  resonances are located at 2.43 and 2.68 MeV, respectively), they govern the behavior of the low-energy  $S$  factor of the  $^{12}\text{C}(\alpha, \gamma)^{16}\text{O}$  reaction (see Ref. [2] and references therein) through the dominating  $E1$  and  $E2$  resonance radiative captures to the ground state of  $^{16}\text{O}$ . Hence, the uncertainties of the subthreshold ANCs should play an important role in the determination of the uncertainty of the total  $S(300 \text{ keV})$  factor.

There are the following important problems regarding the impact of the subthreshold ANCs on the low-energy  $S$  factors. First, the ANCs available in the literature vary quite significantly (see Table I) and the question is how much the variation of the subthreshold ANCs affects the low-energy  $S$  factors. The second problem is the necessity to determine the contribution of the  $1^-$  and  $2^+$  subthreshold resonances (SRs), which are controlled by the subthreshold ANCs, to the total low-energy  $S$  factor, and, in particular,  $S(300 \text{ keV})$

factor. Answering this question will allow us to understand the contribution of the uncertainties of the subthreshold ANCs to the budget of the uncertainty of the low-energy  $S$  factor, especially, the  $S(300 \text{ keV})$  factor. The third problem is to understand the effect of the interference of the SRs with higher resonances and direct capture for the  $E1$  and  $E2$  transitions. Finally, we need to understand the correlated effect of the subthreshold and ground-state ANCs on the low-energy  $S$  factor and, in particular, on the  $S(300 \text{ keV})$  factor.

A novel method was developed and employed in a sequence of papers [19–22] to ascertain the ANCs through extrapolation of elastic scattering phase shifts to subthreshold bound-state poles. Specifically, in Refs. [21,22], this technique was applied to determine the ANCs for  $\alpha$ -particle removal from the four subthreshold states of  $^{16}\text{O}$ :  $0_2^+$ ,  $3^-$ ,  $2^+$ , and  $1^-$ . In this paper, we address all the aforementioned problems by performing comprehensive  $R$ -matrix calculations. We use the subthreshold ANCs found by the extrapolation procedure and the ones taken from Ref. [2], together with two ground-state ANCs of  $^{16}\text{O}$ , a low value of  $58 \text{ fm}^{-1/2}$  [2] and a high value of  $337 \text{ fm}^{-1/2}$  [18].

Unless stated otherwise, we adopt the unit system where  $\hbar = c = 1$ .

## II. METHODOLOGY

### A. Subthreshold resonances

Nuclear excited states below the particle emission threshold (subthreshold states) typically undergo  $\gamma$  decay to lower-lying states. Besides, the presence of the subthreshold states generate a new mechanism of the radiative capture to the low-lying states in which the subthreshold states exhibit themselves as SRs. Below we give a simple explanation of the capture through the SR.

Let us consider two spinless, structureless particles in the continuum forming a bound state by emitting a photon. A very simplified, schematical equation for the amplitude corresponding to the low-energy radiative transition to the ground state is

$$M_{\text{NR}} \sim \langle \varphi_f | \mathcal{H}_{\text{el}}^L | \psi \rangle. \quad (1)$$

<sup>1</sup>The lowest energy at which the  $S$  factor was measured is  $\approx 1 \text{ MeV}$ .

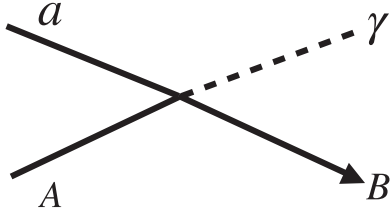


FIG. 1. Diagram describing the nonresonant radiative capture  $^{12}\text{C}(\alpha, \gamma)^{16}\text{O}$ . The short-dashed line represents the emitted photon.

Here  $\psi$  is the scattering wave function,  $\varphi_f$  is the ground bound-state wave function of the interacting particles. The electromagnetic interaction Hamiltonian  $\mathcal{H}_{\text{el}}^L$  is associated with the transition characterized by multipolarity  $L$ .

There are two possible approaches to calculate  $\psi(r)$ . One of them is the two-body potential model, which allows us to simultaneously treat nonresonant, SR and resonance transitions in the given partial wave (see Ref. [23] and the references therein). However, the adopted two-body potential should reproduce simultaneously available experimental scattering phase shifts, binding energies and the corresponding ANCs, and the resonances in the given partial wave. Besides, the two-body potential model may not be good enough to treat the nuclear interior where the many-body approach is required. Also accurate accounting for interference effects continues to be a problem.

The second approach is the  $R$ -matrix formalism, which we utilize in this paper. We underscore the advantages of the  $R$ -matrix method:

- (i) By separating different mechanisms we can explicitly single out the ANCs of the subthreshold bound state and the ground-state ANC as the normalization coefficients of the corresponding amplitudes.
- (ii) Another advantage is that the internal part of the SR radiative amplitude is parametrized in terms of the internal radiative width amplitude which can be calculated using the experimental radiative widths and the channel (external) counterparts or can be a fitting parameter.
- (iii) Finally, the  $R$ -matrix method allows one to take into account the interference effects in a straightforward manner.

We rewrite Eq. (1) in a form convenient for the  $R$ -matrix formalism:

$$M_{\text{NR}} \sim \langle \varphi_f | \mathcal{H}_{\text{el}}^L | I - \mathbb{S} O \rangle, \quad (2)$$

where  $I$  and  $O$  are the incident and outgoing scattered waves in the initial channel,  $\mathbb{S}$  is the elastic scattering  $S$ -matrix element. The diagram shown in Fig. 1 describes the nonresonant radiative capture.

From Eq. (2) one can obtain the radiative capture amplitude proceeding through the SR. The presence of the subthreshold bound state generates a pole in the  $S$ -matrix element at  $E = -\varepsilon_s$ , where  $\varepsilon_s$  is the binding energy of the subthreshold bound state, affecting the second term of the initial scattering wave function in Eq. (2). The impact of the subthreshold bound state

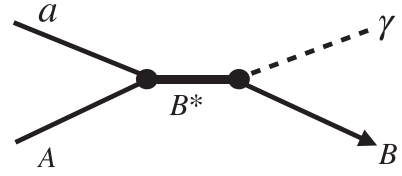


FIG. 2. Pole diagram describing the radiative capture  $^{12}\text{C}(\alpha, \gamma)^{16}\text{O}$  through the SR  $B^*$ . The thick black line is the resonance propagator, the two black spheres are the form factors, and the short-dashed line is the emitted photon.

on the elastic scattering  $S$ -matrix behavior, controlled by a subthreshold pole, becomes more pronounced as the energy approaches zero:

$$\mathbb{S} \stackrel{E \rightarrow +0}{\sim} \frac{\mathcal{A}_s}{E + \varepsilon_s + i \frac{\Gamma(E)}{2}}. \quad (3)$$

The residue in the bound-state pole  $\mathcal{A}_s \sim C_s^2$  [24], where  $C_s$  is the ANC of the subthreshold bound state. However, if we consider the subthreshold bound state as the SR,  $\mathcal{A}_s \sim \Gamma^{\text{SR}}$ , where  $\Gamma^{\text{SR}} \sim C_s^2$  is the width of the SR and  $\Gamma(E) = \Gamma^{\text{SR}}(E) + \Gamma_\gamma(E)$  is the total resonance width of the SR. A tiny radiative width of the SR decaying to the ground state, denoted by  $\Gamma_\gamma(E)$ , will be disregarded in the following discussion. Note that for energy values less than zero,  $\Gamma^{\text{SR}}$  becomes zero due to the presence in it of the penetrability factor, causing the elastic scattering  $S$ -matrix element to exhibit a standard pole behavior,

$$\mathbb{S} \stackrel{E \rightarrow -\varepsilon_s}{\sim} \frac{\mathcal{A}_s}{E + \varepsilon_s}. \quad (4)$$

One can see that for small binding energy  $\varepsilon_s$  the pole term may significantly modify the behavior of the low-energy scattering wave function generating a new mechanism of the radiative capture, namely, the radiative capture “continuum  $\rightarrow$  the ground state” occurring at positive energies of interacting nuclei but contributed by the pole term of the  $S$ -matrix located at the negative energy. This mechanism can be called the radiative capture to the ground state through the SR. Its amplitude can be schematically written as

$$M_{\text{SR}} \sim \frac{\langle \varphi_f | \mathcal{H}_{\text{el}}^L | \sqrt{\Gamma_{\text{SR}}(E)} O \rangle \sqrt{\Gamma_{\text{SR}}(E)}}{E + \varepsilon_s + i \frac{\Gamma_{\text{SR}}(E)}{2}} \quad (5)$$

and is described by the pole diagram shown in Fig. 2. The diagram contains the form factor corresponding to the formation of the SR, resonance propagator and the form factor describing the radiative decay of the SR to the ground state. It has a propagator similar to the real resonance propagator with the resonance energy  $E_R > 0$  replaced by  $-\varepsilon_s$ .

It is now clear that in the presence of the subthreshold bound state the amplitude  $M_{\text{NR}}$  can be written as the sum of two amplitudes:

$$M_{\text{NR}} = M'_{\text{NR}} + M_{\text{SR}}, \quad (6)$$

where the nonresonant radiative capture amplitude  $M'_{\text{NR}}$  is given by

$$M'_{\text{NR}} \sim \langle \varphi_f | \mathcal{H}_{\text{el}}^L | I - S' O \rangle. \quad (7)$$

Here  $\mathbb{S}'$  is the elastic  $S$ -matrix element, which does not contain the bound-state pole. While the initial scattering wave function in the nonresonant radiative transition amplitude  $M_{\text{NR}}^{\text{SR}}$  contains both incident and outgoing waves, the SR amplitude  $M_{\text{SR}}$  contains only the outgoing scattered wave. A distinctive trait of the  $R$ -matrix approach is the partitioning of the radiative capture amplitude into nonresonant and SR segments. The above presented schematic introduction can help the reader to better understand the phenomena of the SRs playing a dominant role in the low-energy radiative capture  $^{12}\text{C}(\alpha, \gamma)^{16}\text{O}$ .

### B. Subthreshold resonances in the $R$ -matrix formalism

The main focus of this paper is to analyze the impact of the subthreshold and ground state ANC on the low-energy  $S$  factor for the radiative capture  $^{12}\text{C}(\alpha, \gamma)^{16}\text{O}$ . The ANC determines the normalization of the peripheral amplitudes. This is the reason we focus on the radiative captures happening in the external (channel) region ( $r > R_{\text{ch}}$ , where  $R_{\text{ch}}$  is the channel radius). This is why utilizing the  $R$ -matrix approach, which separates the configuration space into the internal and channel regions, is advantageous. In the  $R$ -matrix formalism, the calculation of nonresonant (direct) capture to the ground state of the final nucleus only considers the external region, as the nonresonant capture in the internal region is included in the resonance capture amplitude.

There was no mention of the internal and external regions in Eqs. (2)–(7). Nonetheless, a rigorous approach dictates that the internal and channel regions be considered separately. In the  $R$ -matrix approach the total amplitude of the radiative transition to the ground state through the SR is written as the sum of two parts, internal and channel:

$$M_{\text{SR}}(E) = M_{\text{SR}}^{(\text{int})}(E) + M_{\text{SR}}^{(\text{ch})}(E), \quad (8)$$

where

$$M_{\text{SR}}^{(\text{int})}(E) = i e^{i(\sigma_{l_s}^C - \delta_{l_s}^{\text{hs}})} \sqrt{2} (k_{\gamma} R_{\text{ch}})^{L+1/2} \times \frac{\sqrt{\Gamma_{J_s}^{\text{SR}}(E)} \gamma_{\gamma J_0}^{J_s(\text{int})}}{E + \varepsilon_s + i \Gamma_{J_s}^{\text{SR}}(E)/2} \quad (9)$$

is the internal SR radiative transition amplitude and

$$M_{\text{SR}}^{(\text{ch})}(E) = i e^{i(\sigma_{l_s}^C - \delta_{l_s}^{\text{hs}})} \sqrt{2} (k_{\gamma} R_{\text{ch}})^{L+1/2} \times \frac{\sqrt{\Gamma_{J_s}^{\text{SR}}(E)} \gamma_{\gamma J_0}^{J_s(\text{ch})}(E)}{E + \varepsilon_s + i \Gamma_{J_s}^{\text{SR}}(E)/2} \quad (10)$$

is the channel one. Then the total amplitude  $M_{\text{SR}}(E)$  is given by

$$M_{\text{SR}}(E) = i e^{i(\sigma_{l_s}^C - \delta_{l_s}^{\text{hs}})} \sqrt{2} (k_{\gamma} R_{\text{ch}})^{L+1/2} \times \frac{\sqrt{\Gamma_{J_s}^{\text{SR}}(E)} \gamma_{\gamma J_0}^{J_s}(E)}{E + \varepsilon_s + i \Gamma_{J_s}^{\text{SR}}(E)/2}. \quad (11)$$

We explicitly indicated the total angular momentum of the SR  $J_s$  and the total angular momentum of the ground state  $J_0 = 0$ . Since in the case under consideration the channel spin is zero,  $J_s = l_s$ , where  $l_s$  is the orbital angular momentum of the SR, it

is enough to indicate only  $J_s$  or  $l_s$ . Phase shift  $\delta_{l_s}^{\text{hs}}$ , determined by

$$e^{-2i\delta_{l_s}^{\text{hs}}} = \frac{G_{l_s}(k, R_{\text{ch}}) - i F_{l_s}(k, R_{\text{ch}})}{G_{l_s}(k, R_{\text{ch}}) + i F_{l_s}(k, R_{\text{ch}})}, \quad (12)$$

and  $\sigma_{l_s}^C$  are the hard-sphere and Coulomb scattering phase shifts in the partial wave  $l_s$ , respectively. Functions  $F_{l_s}(k, r)$  and  $G_{l_s}(k, r)$  are the regular and irregular Coulomb solutions,  $\Gamma_{J_s}^{\text{SR}}(E)$  and  $\gamma_{\gamma J_0}^{J_s}(E)$  are the observable width and the reduced radiative width amplitude of the SR, respectively.

Even though the SR is situated at negative energy as a subthreshold bound state, its resonance width is specified at  $E > 0$  and vanishes at  $E \leq 0$ :

$$\Gamma_{J_s}^{\text{SR}}(E) = P_{l_s}(k, R_{\text{ch}}) [\gamma_{l_s}^{\text{SR}}(R_{\text{ch}})]^2, \quad (13)$$

where at  $E > 0$  the penetrability factor is

$$P_{l_s}(k, R_{\text{ch}}) = \frac{k R_{\text{ch}}}{F_{l_s}^2(k, R_{\text{ch}}) + G_{l_s}^2(k, R_{\text{ch}})} \quad (14)$$

$$= \frac{k R_{\text{ch}}}{|O_{l_s}(k, R_{\text{ch}})|^2}, \quad (15)$$

$O_{l_s}$  is the outgoing Coulomb scattered wave:<sup>2</sup>

$$O_{l_s}(k, r) = e^{-i\sigma_{l_s}^C} [G_{l_s}(k, R_{\text{ch}}) + i F_{l_s}(k, R_{\text{ch}})] \\ = e^{-i\pi l_s/2} e^{\pi \eta \text{sign}(\text{Re}k)/2} W_{-i\eta, l_s+1/2}(-i2kr), \quad (16)$$

$$\text{sign}(x) = \begin{cases} 1 & \text{for } x > 0, \\ 0 & \text{for } x = 0, \\ -1 & \text{for } x < 0, \end{cases} \quad (17)$$

$W_{-i\eta, l_s+1/2}(-i2kr)$  and  $\eta$  are the Whittaker function and the Coulomb parameter for  $k > 0$ . In addition,

$$[\gamma_{l_s}^{\text{SR}}(R_{\text{ch}})]^2 = \frac{(\hbar c)^2}{\mu} \frac{W_{-\eta_s, l_s+1/2}^2(2\kappa_s R_{\text{ch}})}{R_{\text{ch}}} C_{l_s}^2 \quad (18)$$

is the observable reduced width of the SR, see Appendix A and Refs. [24,26].  $W_{-\eta_s, l_s+1/2}(2\kappa_s R_{\text{ch}})$  is the Whittaker function describing the radial behavior of the bound-state wave function in the external region,  $\kappa_s = \sqrt{2\mu\varepsilon_s}$  is the wave number of the subthreshold bound state,  $\mu$  is the reduced mass of the interacting nuclei expressed in MeV,  $\eta_s$  is the  $\alpha - ^{12}\text{C}$  Coulomb parameter of the subthreshold bound state,  $C_{l_s}$  is the ANC of the subthreshold bound state expressed in  $\text{fm}^{-1/2}$ . We explicitly inserted  $(\hbar c)^2$  in Eq. (18) to validate that  $[\gamma_{l_s}^{\text{SR}}(R_{\text{ch}})]^2$  is measured in MeV. Equation (18) clearly shows that the reduced width of the SR depends only on the ANC  $C_{l_s}$  and the channel radius  $R_{\text{ch}}$ . Hence, the overall normalization of  $\sqrt{\Gamma_{J_s}^{\text{SR}}(E)}$  is expressed in terms of the ANC of the subthreshold bound state  $C_{l_s}$ .

Equation (11) illustrates that the SR is a resonance located at the negative energy of  $-\varepsilon_s$ .  $\gamma_{\gamma J_0}^{J_s(\text{int})}(E)$  and  $\gamma_{\gamma J_0}^{J_s(\text{ch})}(E)$  in Eqs. (9) and (10) are the internal and channel radiative width amplitudes of the SR with the total one,

$$\gamma_{\gamma J_0}^{J_s}(E) = \gamma_{\gamma J_0}^{J_s(\text{int})} + \gamma_{\gamma J_0}^{J_s(\text{ch})}(E). \quad (19)$$

<sup>2</sup>See Ref. [25] for details on how factor  $e^{\pi \eta \text{sign}(\text{Re}k)/2}$  appears.

In the  $R$ -matrix approach  $\gamma_{\gamma J_0}^{J_s(\text{int})}$  is a real constant, while  $\gamma_{\gamma J_0}^{J_s(\text{ch})}(E)$  is complex and energy-dependent.

An explicit expression for  $\gamma_{\gamma J_0}^{J_s(\text{ch})}(E)$  is

$$\begin{aligned} \gamma_{\gamma J_0}^{J_s(\text{ch})}(E) &= C_{l_0} \mathcal{D}_L(E) \sqrt{P_{l_s}(k, R_{\text{ch}})} \gamma_{l_s}^{\text{SR}}(R_{\text{ch}}) \\ &\times \langle l_s, 0, L, 0 | l_0, 0 \rangle U(L, l_0, J_s, s_s; l_s, J_0) \mathcal{J}_{\text{ch}}(E), \end{aligned} \quad (20)$$

where

$$\begin{aligned} \mathcal{D}_L(E) &= \sqrt{\frac{1}{2E}} \frac{1}{(2L+1)!!} \sqrt{\frac{(L+1)(2L+1)}{L}} \\ &\times Z_{\text{eff}}(L) \sqrt{k R_{\text{ch}}} \end{aligned} \quad (21)$$

and (in a concise form)

$$\begin{aligned} \mathcal{J}_{\text{ch}}(E) &= \frac{1}{R_{\text{ch}}^{L+1}} \int_{R_{\text{ch}}}^{\infty} dr r^L W_{-\eta_0, l_0+1/2}(2\kappa_0 r) \\ &\times e^{-i\delta_{l_s}^{\text{bs}}} O_{l_s}(k, r). \end{aligned} \quad (22)$$

$W_{-\eta_0, l_0+1/2}(2\kappa_0 R_{\text{ch}})$  is the Whittaker function describing the external radial behavior of the  $\alpha - {}^{12}\text{C}$  bound-state wave function in the ground state. Subscript  $s$  denotes the continuum state corresponding to the SR, while subscript 0 refers to the ground state of  ${}^{16}\text{O}$ .  $l_0 = 0$ ,  $\kappa_0 = \sqrt{2\mu\varepsilon_0}$  and  $\varepsilon_0 = 7.162$  MeV are the  $\alpha - {}^{12}\text{C}$  orbital angular momentum, bound-state wave number and the binding energy of the  ${}^{16}\text{O}$  ground state, respectively.  $\eta_0$  is the  $\alpha - {}^{12}\text{C}$  Coulomb parameter of the ground bound state. The quantity

$$Z_{\text{eff}}(L) = e\mu^L \left( \frac{Z_\alpha}{m_\alpha^L} + (-1)^L \frac{Z_{12\text{C}}}{m_{12\text{C}}^L} \right) \quad (23)$$

is the effective charge of the system for the transition with multipolarity  $L$ , and  $e$  is the proton charge.

Rewriting this matrix element in terms of the regular  $F_{l_s}(k, r)$  and irregular  $G_{l_s}(k, r)$  Coulomb solutions we get [6]

$$\begin{aligned} \mathcal{J}_{\text{ch}}(E) &= W_{-\eta_0, l_0+1/2}(2\kappa_0 R_{\text{ch}}) \sqrt{F_{l_s}^2(k, R_{\text{ch}}) + G_{l_s}^2(k, R_{\text{ch}})} \\ &\times J_{Ll_s l_0}(E), \end{aligned} \quad (24)$$

where

$$\begin{aligned} J_{Ll_s l_0}(E) &= J_{2Ll_s l_0}(E) \\ &+ i \frac{F_{l_s}(k, R_{\text{ch}}) G_{l_s}(k, R_{\text{ch}})}{F_{l_s}^2(k, R_{\text{ch}}) + G_{l_s}^2(k, R_{\text{ch}})} J_{1Ll_s l_0}(E), \end{aligned} \quad (25)$$

$$\begin{aligned} J_{1Ll_s l_0}(E) &= \frac{1}{R_{\text{ch}}^{L+1}} \int_{R_{\text{ch}}}^{\infty} dr r^L \frac{W_{-\eta_0, l_0+1/2}(2\kappa_0 r)}{W_{-\eta_0, l_0+1/2}(2\kappa_0 R_{\text{ch}})} \\ &\times \left[ \frac{F_{l_s}(k, r)}{F_{l_s}(k, R_{\text{ch}})} - \frac{G_{l_s}(k, r)}{G_{l_s}(k, R_{\text{ch}})} \right], \end{aligned} \quad (26)$$

and

$$\begin{aligned} J_{2Ll_s l_0}(E) &= \frac{1}{R_{\text{ch}}^{L+1}} \int_{R_{\text{ch}}}^{\infty} dr r^L \frac{W_{-\eta_0, l_0+1/2}(2\kappa_0 r)}{W_{-\eta_0, l_0+1/2}(2\kappa_0 R_{\text{ch}})} \\ &\times \left[ \frac{F_{l_s}(k, r) F_{l_s}(k, R_{\text{ch}}) + G_{l_s}(k, r) G_{l_s}(k, R_{\text{ch}})}{F_{l_s}^2(k, R_{\text{ch}}) + G_{l_s}^2(k, R_{\text{ch}})} \right]. \end{aligned} \quad (27)$$

Then

$$\begin{aligned} \gamma_{\gamma J_0}^{J_s(\text{ch})}(E) &= C_{l_0} \sqrt{k R_{\text{ch}}} \mathcal{D}_L(E) \gamma_{l_s}^{\text{SR}}(R_{\text{ch}}) \\ &\times \langle l_s, 0, L, 0 | l_0, 0 \rangle U(L, l_0, J_s, s_s; l_s, J_0) \\ &\times W_{-\eta_0, l_0+1/2}(2\kappa_0 R_{\text{ch}}) J_{Ll_s l_0}(E). \end{aligned} \quad (28)$$

$C_{l_0}$  is the ANC of the  ${}^{16}\text{O}$  ground state,  $Z_i$  is the number of the protons in nucleus  $i$ ,  $k_\gamma = E + \varepsilon_0$  is the momentum of the emitted photon,  $k = \sqrt{2\mu E}$ ,  $\langle l_s, 0, L, 0 | l_0, 0 \rangle$  is the Clebsch-Gordan coefficient,  $U(L, l_0, J_s, s_s; l_s, J_0)$  is the Racah coefficient,  $s_s = 0$  is the  $\alpha - {}^{12}\text{C}$  channel spin in the subthreshold state.

For the bound states  $J_{Ll_s l_0}$  is given by [6]

$$\begin{aligned} J_{Ll_s l_0} &= \frac{1}{R_{\text{ch}}^{L+1}} \int_{R_{\text{ch}}}^{\infty} dr r^L \frac{W_{-\eta_0, l_0+1/2}(2\kappa_0 r)}{W_{-\eta_0, l_0+1/2}(2\kappa_0 R_{\text{ch}})} \\ &\times \frac{W_{-\eta_s, l_s+1/2}(2\kappa_s r)}{W_{-\eta_s, l_s+1/2}(2\kappa_s R_{\text{ch}})}. \end{aligned} \quad (29)$$

The channel radiative width pertaining to the bound state is given by

$$\begin{aligned} \gamma_{\gamma J_0}^{J_s(\text{ch})}(-\varepsilon_s) &= \sqrt{2\mu} Z_{\text{eff}}(L) R_{\text{ch}} \frac{1}{(2L+1)!!} \\ &\times \sqrt{\frac{(L+1)(2L+1)}{L}} C_{l_0} W_{-\eta_0, l_0+1/2} \\ &\times (2\kappa_0 R_{\text{ch}}) \langle l_s, 0, L, 0 | l_0, 0 \rangle \\ &\times U(L, l_0, J_s, s_s; l_s, J_0) \gamma_{J_s}(R_{\text{ch}}) J_{Ll_s l_0}, \end{aligned} \quad (30)$$

where  $\gamma_{J_s}(R_{\text{ch}})$  is the reduced width of the subthreshold bound state, which is expressed in terms of the subthreshold ANC  $C_{J_s}$ .

We see that the normalization of the channel radiative width is expressed in terms of the subthreshold ANC  $C_{l_s}$  and the ANC  $C_{l_0}$  of the ground state of  ${}^{16}\text{O}$ . It explains why these ANCs govern the behavior of the low-energy amplitude  $M_{\text{SR}}^{(\text{ch})}(E)$  describing the channel resonance radiative transition to the ground state through the SR.

The radiative width of the SR is expressed in terms of  $\gamma_{\gamma J_0}^{J_s}(E)$  as

$$\begin{aligned} \Gamma_{\gamma J_0}^{J_s}(E) &= 2(k_\gamma R_{\text{ch}})^{2L+1} \left| \gamma_{\gamma J_0}^{J_s}(E) \right|^2 \\ &= 2(k_\gamma R_{\text{ch}})^{2L+1} \left| \gamma_{\gamma J_0}^{J_s(\text{int})} + \gamma_{\gamma J_0}^{J_s(\text{ch})}(E) \right|^2. \end{aligned} \quad (31)$$

If  $|\gamma_{\gamma J_0}^{J_s(\text{int})}| \gg |\gamma_{\gamma J_0}^{J_s(\text{ch})}(E)|$ , then the energy dependence of  $\Gamma_{\gamma J_0}^{J_s}(E)$  is determined by the dimensionless factor  $(k_\gamma R_{\text{ch}})^{2L+1}$  and we can write

$$\Gamma_{\gamma J_0}^{J_s}(E) = \left( \frac{E + \varepsilon_0}{\varepsilon_0 - \varepsilon_s} \right)^{2L+1} \Gamma_{\gamma J_0}^{J_s}(-\varepsilon_s). \quad (33)$$

This equation allows one to find the radiative width  $\Gamma_{\gamma J_0}^{J_s}(E)$  at positive energies if (it is often the case)  $\Gamma_{\gamma J_0}^{J_s}(-\varepsilon_s)$  is known experimentally.

We remind that  $\gamma_{\gamma J_0}^{J_s(\text{ch})}(E)$  can be explicitly calculated. If its energy dependence is weak, then Eq. (33) can be a good approximation even for the nonnegligible channel part. Then, in view of Eq. (32), one can find  $\gamma_{\gamma J_0}^{J_s(\text{int})}$ :

$$\gamma_{\gamma J_0}^{J_s(\text{int})} = -\text{Re}\gamma_{\gamma J_0}^{J_s(\text{ch})}(E) \pm \sqrt{\frac{\Gamma_{\gamma J_0}^{J_s}(E)}{2(k_\gamma R_{\text{ch}})^{2L+1}} - [\text{Im}\gamma_{\gamma J_0}^{J_s(\text{ch})}(E)]^2}. \quad (34)$$

### C. Direct radiative capture

There is another radiative process where the subthreshold bound states contribute: the cascade radiative capture to the ground state through the subthreshold bound states. It is a two-step process, which begins with the first direct radiative capture to the subthreshold bound state, which is then followed by its decay to the ground state through photon emission. The direct capture amplitude to the subthreshold state, which is the first part of the cascade transition to the ground state, is given by

$$\mathcal{M}_{\text{DC}(s)}(E) = e^{i(\sigma_i^c - \delta_i^{\text{hs}})} \sqrt{2} \mathcal{D}_L(E) (k_\gamma R_{\text{ch}})^{L+1/2} C_{l_s} \times \langle l_i 0 L 0 | l_s 0 \rangle U(L l_s J_i s_i; l_i J_s) \mathcal{J}_{is}(E), \quad (35)$$

with

$$\mathcal{J}_{is}(E) = \frac{1}{R_{\text{ch}}^{L+1}} \int_{R_{\text{ch}}}^{\infty} dr r^L W_{-\eta_s, l_s+1/2}(2\kappa_s r) \times [e^{i\delta_i^{\text{hs}}} I_l(k, r) - e^{-i\delta_i^{\text{hs}}} O_l(k, r)]. \quad (36)$$

Here  $l_i$  is the  $\alpha$ - $^{12}\text{C}$  orbital angular momentum in the continuum,  $s_i = 0$  is their channel spin.

Rewriting  $\mathcal{J}_{is}(E)$  in terms of the regular and irregular Coulomb solutions we get [6]

$$\mathcal{J}_{is}(E) = 2i W_{-\eta_s, l_s+1/2}(2\kappa_s R_{\text{ch}}) \times \frac{F_l(k, R_{\text{ch}}) G_l(k, R_{\text{ch}})}{\sqrt{F_l^2(k, R_{\text{ch}}) + G_l^2(k, R_{\text{ch}})}} J_{1Ll_l s}(E). \quad (37)$$

Equation (35) clarifies why in the  $R$ -matrix approach the overall normalization of the direct capture amplitude is determined by the ANC of the final bound state formed as the result of the direct radiative capture [25].

We explicitly showed only the amplitude of the first step of the cascade radiative capture. For the subthreshold case under consideration, the cascade transitions through (7.12 MeV,  $1^-$ ) and (6.92 MeV,  $2^+$ ) subthreshold bound states are significantly weaker than the resonant captures to the ground state when these bound states reveal themselves as the SRs (see Fig. 4). In addition to direct capture to the subthreshold bound state, it is necessary to consider the direct ‘‘continuum-to-ground-state’’ capture. The amplitude of this transition is similar to the amplitude  $\mathcal{M}_{\text{DC}(s)}(E)$  [see Eq. (35)] and is given by

$$\mathcal{M}_{\text{DC}(0)}(E) = e^{i(\sigma_i^c - \delta_i^{\text{hs}})} \mathcal{D}_L(E) (k_\gamma R_{\text{ch}})^{L+1/2} C_0 \times \langle l_i 0 L 0 | l_0 \rangle U(L l_0 J_i s_i; l_i J_0) \mathcal{J}_{i0}(E). \quad (38)$$

The formula for  $\mathcal{J}_{i0}(E)$  can be derived from  $\mathcal{J}_{is}(E)$  [refer to Eq. (36)] by substituting subscript  $s$  with 0. Note that the only unknown quantity in Eq. (38) is the ANC  $C_0$  of the ground state of  $^{16}\text{O}$ . This ANC can be positive or negative<sup>3</sup> determining the sign of  $\mathcal{M}_{\text{DC}(0)}(E)$ . For  $l_i = l_s$  the direct capture amplitude  $\mathcal{M}_{\text{DC}(0)}(E)$  interferes with the amplitude  $M_{\text{SR}}(E)$  for the resonance capture to the ground state through the SR. The sign of Eq. (28) and, hence, of  $M_{\text{SR}}(E)$  is controlled by the product  $C_{l_0} C_{l_s}$ . If we fix the sign of the subthreshold ANC  $C_{l_s}$ , then the nonresonant amplitude  $\mathcal{M}_{\text{DC}(0)}(E)$  and the channel resonance radiative amplitude  $M_{\text{SR}}^{\text{(ch)}}(E)$  are normalized in terms of the same ANC,  $C_0$ . Such a normalization is physically transparent: both amplitudes describe peripheral processes and, hence, contain the tail of the nuclear overlap function of the ground state, whose normalization is given by the corresponding ANC.

For the interfering direct capture to the ground state and the resonance capture to the ground state through the SR, it is convenient to write the sum of the interfering amplitudes as

$$M_{\text{SR}}(E) + \mathcal{M}_{\text{DC}(0)}(E) = [M_{\text{SR}}^{\text{(ch)}}(E) + \mathcal{M}_{\text{DC}(0)}(E)] + M_{\text{SR}}^{\text{(int)}}(E). \quad (39)$$

The relative sign of the sum in the brackets is well determined, while the sign of  $M_{\text{SR}}^{\text{(int)}}(E)$ , which contains  $\gamma_{\gamma J_0}^{J_s(\text{int})}$ , is the fitting parameter.

The equations in this section shed light on the reason behind the extensive effort dedicated to determining the ANCs of the  $\alpha$ -particle removal from the subthreshold bound states of  $^{16}\text{O}$  (see Ref. [2]). The different experimental and theoretical methods of determining the ANCs are discussed in Ref. [25].

### D. Resonant transition

Since the main purpose of this paper is to investigate the role of the subthreshold ANCs, we only briefly discuss the resonance capture to the ground state of  $^{16}\text{O}$ . Equations for the resonance capture can be obtained from the corresponding equations for resonance capture through the SR by replacing  $s \rightarrow i$ ,  $-\varepsilon_s \rightarrow E_R$ , where  $E_R$  is the resonance energy,<sup>4</sup>  $\Gamma_s^{\text{SR}}(E) \rightarrow \Gamma_i(E)$  and  $\gamma_{\gamma J_0}^{J_s}(E) \rightarrow \gamma_{\gamma J_0}^{J_i}(E)$ . Here  $\Gamma_i(E)$  is the resonance width,  $\gamma_{\gamma J_0}^{J_i}(E)$  is the resonance radiative width amplitude, which can be split into the internal and channel parts, and  $l_i$  is  $\alpha$ - $^{12}\text{C}$  resonance orbital angular momentum. For  $l_i = l_s$  the resonance amplitude interferes with the SR and direct capture amplitudes. Adding higher resonances interfering with the SR requires employing the multilevel  $R$ -matrix equations [2,8].

### E. ANC of the ground state of $^{16}\text{O}$

Here we discuss the impact of the ground state ANC  $C_0$ . This ANC enters the channel radiative widths of the SR and

<sup>3</sup>By definition, the ANC is a real quantity.

<sup>4</sup>The  $R$ -matrix approach deals only with real resonance energies.

the resonance, cascade transition and direct capture amplitudes to the ground state. Owing to the large binding energy of the ground state of the system  $\alpha + {}^{12}\text{C}$  ( $\varepsilon_0 = 7.16$  MeV), the internal part of the radiative width of the SR  $\gamma_{\gamma J_0}^{J_s(\text{int})}(E)$  and the resonance internal radiative width  $\gamma_{\gamma J_0}^{J_s(\text{int})}(E)$  are dominant compared to the corresponding channel ones containing  $C_{l_0}$ . Besides, for the  $E1$  transition the channel part is suppressed because the effective charge  $Z_{\text{eff}}(1)$  is very small ( $Z_{\text{eff}}(1)/e = -0.00097$ ). It significantly diminishes the role of the channel radiative widths. For the same reason, the  $E1$  direct capture to the ground state is suppressed. The numerical evidence provided below indicates that the ground-state ANC has no influence on the  $E1$   $S(300$  keV) factor at low energies.

Also the cascade transitions to the ground state are small compared to the SR and resonance transitions. It makes the impact of the ground-state ANC less important than that of the ANCs of the subthreshold states  $1^-$  and  $2^+$ , but not negligible due to the interference of the  $2^+$  SR, resonance and the direct transition to the ground state. The role of  $C_{l_0}$  on the low-energy  $S$  factor, especially,  $S(300$  keV), is analyzed through numerical calculations below. Two sets of subthreshold ANCs from the low end [2] and high end [22] are used in this paper for systematic comparison. The latter set was determined using the extrapolation procedure of the elastic scattering phase shifts. However, the ground-state ANC was not determined using the extrapolation method because it is located quite far from the threshold (the binding energy of the  $\alpha$  particle in the  ${}^{16}\text{O}$  ground state is 7.16 MeV). The values of the ground-state ANC published in the literature vary significantly [18]. In this paper, we explore two values of this ANC:  $58$  fm $^{-1/2}$  [2] and  $337$  fm $^{-1/2}$  [18]. The ground-state ANC of  $337 \pm 45$  fm $^{-1/2}$  found in Ref. [18] from the heavy-ion-induced transfer reaction requires a higher value of  $(1.55 \pm 0.09) \times 10^5$  fm $^{-1/2}$  for the ANC of the ( $2^+$ , 6.92 MeV) excited state to reconcile with the  $S$  factor from Ref. [2] calculated for the ground-state ANC of  $58$  fm $^{-1/2}$ . This value of the  $2^+$  subthreshold ANC is close but slightly higher than the ANC for the 6.92 MeV state from Ref. [22] (see Table I).

### F. Subthreshold ANCs

One of the main goals of this paper is to check the impact of the ANCs of the  $\alpha$ -particle removal from the subthreshold states  $1^-$  and  $2^+$  of  ${}^{16}\text{O}^*$ . The ANCs of these subthreshold bound states available in the literature have been recently tabulated in Ref. [2]. This revealed large discrepancies between the ANCs determined by different techniques, suggesting further efforts are needed to pinpoint the ANCs of the two near-threshold bound states in  ${}^{16}\text{O}$ . The ANC values for the channels  ${}^{16}\text{O}^* \rightarrow \alpha + {}^{12}\text{C}$  obtained by various methods are also compared in Table I.

It is not the goal of this paper to verify the reliability and uncertainty of each subthreshold ANC published in the literature. To assess the effects of the subthreshold ANCs, as previously mentioned, we will be analyzing two sets: one represents the lower end of the published subthreshold ANCs and is taken from Ref. [2], while the second set representing the high-end of the subthreshold ANCs was reported recently (the last two rows in Table I, which are taken from Refs. [21,22]).

TABLE II. Channel and internal radiative width amplitudes for the SR  $1^-$ .

$E$ (MeV)	$\gamma_{\gamma 0}^{1(\text{ch})}(E)$ (MeV $^{1/2}$ )	$\gamma_{\gamma 0}^{1(m)}(\text{int})$ (MeV $^{1/2}$ )	$\gamma_{\gamma 0}^{1(p)}(\text{int})$ (MeV $^{1/2}$ )
0.1	$3.20 \times 10^{-8} + i 7.16 \times 10^{-30}$	-0.00146	0.00146
0.2	$3.22 \times 10^{-8} + i 1.2 \times 10^{-21}$	-0.00146	0.00146
0.3	$3.25 \times 10^{-8} + i 4.97 \times 10^{-18}$	-0.00146	0.00146
0.4	$3.28 \times 10^{-8} + i 6.75 \times 10^{-16}$	-0.00146	0.00146
0.5	$3.32 \times 10^{-8} + i 1.85 \times 10^{-14}$	-0.00146	0.00146

The ANCs obtained in Refs. [21] and [22] were obtained by the extrapolation of the experimental phase shifts in the corresponding partial waves to the subthreshold bound-state poles located at negative energies. Unfortunately, uncertainties of the experimental phase shifts are unknown. Therefore, in this paper, to estimate uncertainties of the ANCs obtained by the extrapolation method we assumed 5% uncertainty in the experimental phase shifts.

To be consistent we included in our calculations all four subthreshold states in  ${}^{16}\text{O}$ , although we understand that only  $1^-$  and  $2^+$  give the dominant contribution. Note that the uncertainty of the ANC for the  $0_2^+$  state determined by applying the extrapolation method is significantly higher than for the three weaker bound subthreshold states presented in Table I. The reason is that the farther the threshold state from the pole that corresponds to the bound state in the energy plane, the lower is the accuracy of the ANC obtained by the extrapolation of the elastic-scattering phase shifts to the corresponding bound-state pole.

### G. Radiative width amplitudes of the subthreshold resonances $1^-$ and $2^+$

The amplitudes  $M_{\text{SR}}(E)$  of the radiative capture  ${}^{12}\text{C}(\alpha, \gamma){}^{16}\text{O}$  through the  $1^-$  and  $2^+$  SRs give the dominant contribution to the low-energy  $S$  factors. These amplitudes depend on the resonance widths of SRs  $\Gamma_{J_s}^{\text{SR}}(E)$ , which can be calculated explicitly, and the radiative width amplitudes  $\gamma_{\gamma J_0}^{J_s}(E)$  of the SRs. Before presenting the results of the low-energy  $S$  factor calculations, we will review the SR radiative widths amplitudes.

#### 1. Subthreshold resonance $1^-$

First, we consider the radiative width amplitude for the SR  $1^-$ . Owing to the fact the ratio  $Z_i/m_i$  for the  $\alpha$  particle and  ${}^{12}\text{C}$  is practically the same, the effective charge for the  $L = 1$  transition is very small and the channel radiative width amplitude  $\gamma_{\gamma J_0}^{J_s(\text{ch})}(E)$  should be negligible compared to the internal counterpart.<sup>5</sup> In Table II are shown the low-energy dependencies of the channel and internal radiative

<sup>5</sup>Each of involved nuclei,  ${}^4\text{He}$  and  ${}^{12}\text{C}$  have  $Z_i = N_i$ , where  $N_i$  is the number of neutrons in nucleus  $i$ . For systems with such nuclei the isospin projection  $T_3 = 0$  and the isospin selection rule requires change of the isospin of the system by one. Since it is not fulfilled in our case, the considered  $E1$  transition  $1^- \rightarrow 0^+$  is called isospin

TABLE III. Channel and internal radiative width amplitudes for the SR  $2^+$ .

$E$ (MeV)	$\gamma_{\gamma 0}^{2(ch)}(E)$ ( $\text{MeV}^{1/2}$ )	$\gamma_{\gamma 0}^{2(m)}(\text{int})$ ( $\text{MeV}^{1/2}$ )	$\gamma_{\gamma 0}^{1(p)}(\text{int})$ ( $\text{MeV}^{1/2}$ )
0.1	$1.5 \times 10^{-5} + i 8.13 \times 10^{-28}$	-0.0089	0.0089
0.2	$1.5 \times 10^{-5} + i 1.43 \times 10^{-19}$	-0.0089	0.0089
0.3	$1.5 \times 10^{-5} + i 6.19 \times 10^{-16}$	-0.0089	0.0089
0.4	$1.5 \times 10^{-5} + i 8.81 \times 10^{-14}$	-0.0089	0.0089
0.5	$1.5 \times 10^{-5} + i 2.53 \times 10^{-12}$	-0.0089	0.0089

width amplitudes for the SR  $1^-$ . Just as anticipated, the inner component is unchanging. We can see that the internal part is significantly larger than the channel part, leading to the validity of Eq. (33). The experimental value of the radiative width of the subthreshold bound state  $1^-$  decaying to the ground state is  $\Gamma_{\gamma 0}^1(-0.045 \text{ MeV}) = (5.5 \pm 0.3) \times 10^{-8} \text{ MeV}$  [34]. Hence, the internal radiative width amplitude can be calculated using Eqs. (33) and (34). A 6% experimental uncertainty of  $\Gamma_{\gamma 0}^1(-0.045 \text{ MeV})$  propagates into the 3% uncertainty of  $\gamma_{\gamma 0}^1(\text{int})$ .  $\gamma_{\gamma 0}^1(\text{int})[\gamma_{\gamma 0}^1(\text{int})]$  in Table II corresponds to the higher (lower) solution of Eq. (34). For practical calculations we use  $\gamma_{\gamma 0}^1(\text{int}) = (1.46 \pm 0.05) \times 10^{-3} \text{ MeV}^{1/2}$ . It should be noted that even for the high subthreshold ANC (the last row of Table I) and the high ground-state ANC of  $337 \text{ fm}^{-1/2}$  [18] the channel radiative width amplitude  $\gamma_{\gamma 0}^{1(ch)}(300 \text{ keV}) = 2.06 \times 10^{-7} + i 3.15 \times 10^{-17} \text{ MeV}^{1/2}$  remains negligible compared to the internal counterpart, which does not depend on the ANCs.

## 2. Subthreshold resonance $2^+$

Although for  $L = 2$  the effective charge is not small, due to the high binding energy of the ground state of  $^{16}\text{O}$ ,  $\gamma_{\gamma 0}^2(\text{ch})$  is significantly smaller than  $\gamma_{\gamma 0}^2(\text{int})$ , see Table III. Hence, Eq. (33) is also applicable for  $L = 2$ . The experimental value of the radiative width of the subthreshold bound state  $2^+$  decaying to the ground state is  $\Gamma_{\gamma 0}^2(-0.245 \text{ MeV}) = (9.7 \pm 0.3) \times 10^{-8} \text{ MeV}$  [34]. Again, as it was for the  $1^-$  subthreshold state, Eqs. (33) and (34) are used to calculate the internal radiative width amplitudes (notations are the same as in Table II). A 3% uncertainty of  $\Gamma_{\gamma 0}^2(-0.245 \text{ MeV})$  propagates to 1.5% uncertainty of  $\gamma_{\gamma 0}^2(\text{int})$ . For calculations we use  $\gamma_{\gamma 0}^{2(p)}(\text{int}) = 0.0089 \pm 0.0001 \text{ MeV}^{1/2}$ . It should be underscored that for the high subthreshold ANC for the  $2^+$  state (the last row of Table I) and the high ground-state ANC of  $337 \text{ fm}^{-1/2}$  [18] the channel radiative width amplitude  $\gamma_{\gamma 0}^{2(ch)}(300 \text{ keV}) = 1.63 \times 10^{-3} + i 6.67 \times 10^{-14} \text{ MeV}^{1/2}$  remains small but not negligible compared to the internal counterpart.

forbidden [35,36]. However, the suppression is not very strict because of the mass difference between the protons and neutrons and the residual Coulomb effects.

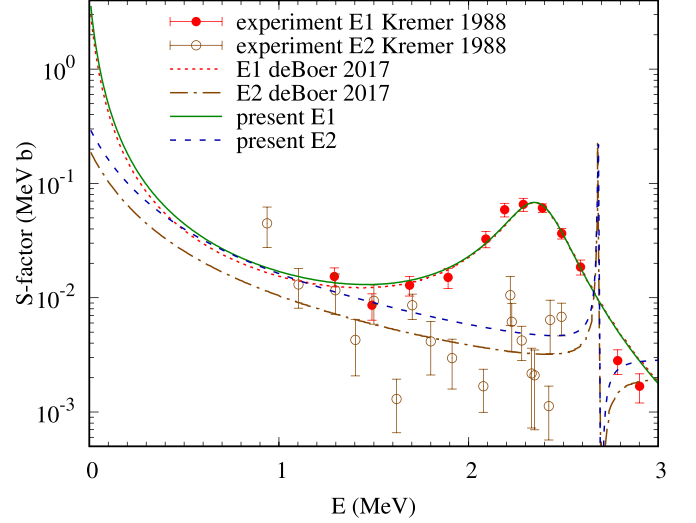


FIG. 3.  $S$  factors for the  $^{12}\text{C}(\alpha, \gamma)^{16}\text{O}$  radiative capture reaction to the ground state through the  $1^-$  and  $2^+$  resonances. The solid and open circles are experimental data from Kremer *et al.* [5] for the  $E1$  and  $E2$  transitions, respectively. The dotted and dash-dotted lines are the  $S$  factors from deBoer *et al.* [2] for the resonance  $E1$  and  $E2$  transitions, respectively. The solid and dashed lines are the resonance  $S$  factors for the  $E1$  and  $E2$  transitions obtained using our ANCs (see the last row of Table I).

## III. S-FACTORS FOR $^{12}\text{C}(\alpha, \gamma)^{16}\text{O}$ RADIATIVE CAPTURE TO THE GROUND STATE OF $^{16}\text{O}$

### A. $S$ factors for resonance $E1$ and $E2$ captures to the ground state

First we present the results of the calculations for two dominant low-energy  $S$  factors corresponding to the resonance  $E1$  and  $E2$  transitions to the ground state. The resonance  $E1$  transition is made of contributions from the SR (7.12 MeV,  $1^-$ ), the first above the threshold resonance (9.59 MeV,  $1^-$ ), and higher  $1^-$  resonances. Similarly, the resonance  $E2$  transition is dominated by the SR (6.92 MeV,  $2^+$ ), the lowest above-threshold resonance (9.85 MeV,  $2^+$ ) and higher  $2^+$  resonances.

Although below for convenience we show the  $S$  factors for the radiative capture  $^{12}\text{C}(\alpha, \gamma)^{16}\text{O}$  for energies  $E < 3 \text{ MeV}$ , our main focus is the low-energy region  $E < 1 \text{ MeV}$ , and especially the most effective astrophysical energy  $E = 300 \text{ keV}$ , at which we can check the impact of the subthreshold ANCs on the  $S(300 \text{ keV})$  factors. We compare the  $S$  factors calculated using the central values of the ANCs in the last row of Table I with the results from the review [2]. In this energy region it is enough to take into account the two lowest levels (the SR and the lowest resonance at  $E > 0$ ) in addition to background resonances for the  $E1$  and  $E2$  resonance transitions. Details and parameters used in the calculations are given in Ref. [2].

Thus the resonance  $E1$  and  $E2$   $S$  factors depicted in Fig. 3 are calculated for the subthreshold ANCs  $2.08 \times 10^{14} \text{ fm}^{-1/2}$  [for the (7.12 MeV,  $1^-$ )] and  $1.14 \times 10^5 \text{ fm}^{-1/2}$  [for the (6.92 MeV,  $2^+$ )] from Ref. [2], which are compared with the higher sets of the ANCs,  $2.27 \times 10^{14} \text{ fm}^{-1/2}$  and  $1.42 \times$

TABLE IV. Comparison of the current  $S$  factors and the  $S$  factors from Ref. [2] for transition to the ground state of  $^{16}\text{O}$  at the most effective astrophysical energy of 300 keV. The resonance  $E1$  and  $E2$  transitions include interference with the direct  $E1$  and  $E2$  captures to the ground state. The cascade transition is the radiative capture to the ground state proceeding through four subthreshold bound states of  $^{16}\text{O}$ :  $0_2^+$ ,  $3^-$ ,  $2^+$ , and  $1^-$ . We remind that all the calculations were done for the low ground-state ANC of  $58 \text{ fm}^{-1/2}$ . The  $S$  factors are given in units of keVb.

Transition to the ground state via resonance + direct capture	$S(300 \text{ keV})$ Present	$S(300 \text{ keV})$ Ref. [2]
$E1$	98	85
$E2$	70	45
$E1 + E2$	168	130
Cascade	Present	Ref. [2]
$0_2^+ + 3^- + 2^+ + 1^-$	6	7
Total	Present	Ref. [2]
$E1 + E2 + \text{cascade}$	174	137

$10^5 \text{ fm}^{-1/2}$  [22] (the last row of Table I). It can be seen that as the values of the subthreshold ANCs increase, both  $E1$  and  $E2$   $S$  factors exhibit an increase. The exact values of the calculated resonance  $E1$  and  $E2$   $S$  factors at 300 keV are given in Table IV. We need to add some additional comments about the calculation of the  $E1$  and  $E2$  resonance captures to the ground state of  $^{16}\text{O}$ . Precisely speaking, we accounted for the interference of the  $E1$  and  $E2$  resonance captures to the ground state with the  $E1$  and  $E2$  direct captures to the ground state. Shown in Fig. 3  $E1$  and  $E2$   $S$  factors include all the transitions to the ground state except for the cascade transitions, which are discussed in Sec. III B. In the calculations shown in Fig. 3 we adopted a low value of the ground-state ANC  $C_0 = 58 \text{ fm}^{-1/2}$  taken from Ref. [2], because our goal was to compare with the results from Ref. [2] by varying only the subthreshold ANCs.

### B. Radiative capture to subthreshold states and the total $S$ factor for $^{12}\text{C}(\alpha, \gamma)^{16}\text{O}$ radiative capture

Besides the  $E1$  and  $E2$  resonance captures to the ground state, we also calculated the cascade transitions to the ground state through the four excited bound states (6.05 MeV,  $0_2^+$ ), (6.13 MeV,  $3^-$ ), (6.92 MeV,  $2^+$ ), and (7.12 MeV,  $1^-$ ) using the ANCs from the last two rows of Table I. The cascade transitions to the ground state of  $^{16}\text{O}$  represent two-step processes: the direct capture to one of the excited states is followed by the radiative decay of the excited bound state to the ground state. The ANCs of the four subthreshold bound states under consideration govern the normalization of the direct capture amplitudes.

Figure 4 depicts all the  $S$  factors calculated using the ANCs obtained by the extrapolation procedure. In this figure we show not only the  $S$  factors for the cascade transition through the four excited states of  $^{16}\text{O}$  but also the  $S$  factors for the  $E1$  and  $E2$  resonance captures to the ground state of  $^{16}\text{O}$  (see Fig. 3) and the total  $S$  factor, which is the sum of all six  $S$  factors shown in Fig. 4.

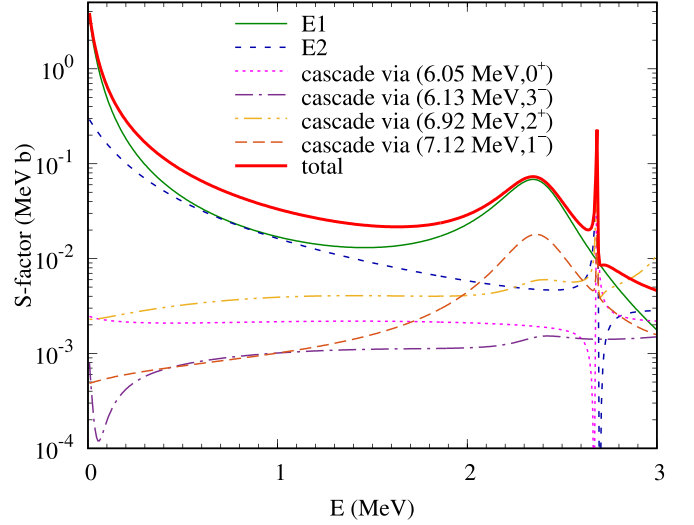


FIG. 4. All the calculated  $S$  factors for radiative captures to the ground state. The  $S$  factors for the  $E1$  and  $E2$  resonance radiative captures to the ground state, which interfere with the corresponding direct captures, are presented by thin solid and short-dashed lines, respectively. The  $S$  factors for the cascade radiative captures to the ground state through the 7.12 MeV state—long-dashed line; the radiative capture through the 6.92 MeV state—dot-dot-dashed line; the radiative capture through the 6.13 MeV state—dot-dashed line, the radiative capture through the 6.05 MeV state—dotted line. The thick solid line is the total  $S$  factor given by the sum of all the  $S$  factors shown in this figure.

### IV. CORRELATION BETWEEN THE SUBTHRESHOLD ANCS AND THE TOTAL $E1$ AND $E2$ $S$ FACTORS

The results of the comparison of the  $S$  factors from the current paper and the ones from Ref. [2] are presented in Table IV. The difference between them is caused by variation of only one parameter, the ANC of the corresponding subthreshold state. It is evident that the rise in subthreshold state ANCs leads to an increase in the  $E1$  and  $E2$   $S(300 \text{ keV})$  factors.

Table V shows the correlation between the variations of the ANCs of the subthreshold bound states causing the corresponding variations  $S(300 \text{ keV})$  factors. In this table  $\Delta C_i^2 = C_{i(\text{pr})}^2 / C_{i(\text{RMP})}^2 - 1$  and  $\Delta S(300 \text{ keV}) = S_{\text{pr}}(300 \text{ keV}) / S_{\text{RMP}}(300 \text{ keV}) - 1$ . Quantities with the subscript “pr” are calculated using the present ANCs and those with the subscript “RMP” use ANCs from Ref. [2]. We observe around 79% correlation between the uncertainties of the ANC for the  $1^-$  subthreshold state and of the total  $S_{E1}(300 \text{ keV})$  factor for the  $E1$  transition to the ground

TABLE V. Correlation between the uncertainties of squares of ANCs and the  $S(300 \text{ keV})$  factors.

Transitions	$\Delta C_i^2, \%$	$\Delta S(300 \text{ keV}), \%$
$E1$	19	15
$E2$	55	56
$E1 + E2$		29

TABLE VI.  $S(300\text{ keV})$  factors (expressed in keVb) for the radiative capture  $^{12}\text{C}(\alpha, \gamma)^{16}\text{O}$  presented in Figs. 5–7. The first column pertains to the figure displaying the relevant results.  $S_{E1}$  and  $S_{E2}$  are the total  $S$  factors for the  $E1$  and  $E2$  transitions,  $S_{E1+E2} = S_{E1} + S_{E2}$ .  $S_{E1}^{(\text{SR})}$  and  $S_{E2}^{(\text{SR})}$  are the  $S(300\text{ keV})$  factors for the resonance  $E1$  and  $E2$  transitions through the SRs  $1^-$  and  $2^+$  only.  $S_{E1}^{(\text{SR})}/S_{E1}$  and  $S_{E2}^{(\text{SR})}/S_{E2}$  are the ratios of the corresponding  $S$  factors.

Fig.	$S_{E1+E2}$	$S_{E1}$	$S_{E2}$	$S_{E1}^{(\text{SR})}$	$S_{E2}^{(\text{SR})}$	$S_{E1}^{(\text{SR})}/S_{E1}$	$S_{E2}^{(\text{SR})}/S_{E2}$
5	130	85	45	60	46	0.71	1.02
6	168	98	70	72	72	0.74	1.03
7	155	99	56	72	72	0.73	1.29

state of  $^{16}\text{O}$ . An additional contribution to the  $E1$  transition may come from interference between the  $1^-$  SR with the higher broad ( $E_X = 9.59\text{ MeV}$ ;  $1^-$ ) MeV resonance and the direct capture to the ground state.<sup>6</sup> Thus, a 5% uncertainty of the subthreshold ANC  $C_1$  generates about 4% uncertainty of the total  $E1$   $S(300\text{ keV})$  factor. As previously discussed, the  $E1$   $S_{E1}(300\text{ keV})$  factor is independent of the ground-state ANC, as illustrated in Table VI below. Hence, the interference of the  $E1$  SR occurs only with the broad 9.59 MeV resonance.

For the  $E2$  transition we get almost 100% correlation between the subthreshold ANC for the subthreshold  $2^+$  state and the  $S_{E2}(300\text{ keV})$  factor for the  $E2$  transition to the ground state. We can conclude that at low ground-state ANC of  $58\text{ fm}^{-1/2}$ , the interference effect of the subthreshold  $2^+$  resonance with higher resonance and the direct capture amplitudes is negligible. Hence, when other parameters are fixed, the uncertainty of the subthreshold ANC for the  $2^+$  state almost completely propagates into the uncertainty of the  $S_{E2}(300\text{ keV})$  for the  $E2$  radiative captures to the ground state. Accordingly, for the low ground-state ANC, a 5% uncertainty of the subthreshold ANC  $C_2$  generates about 5% uncertainty in the total  $S_{E2}(300\text{ keV})$  factor.

## V. LOW-ENERGY $S$ FACTORS FOR RESONANCE CAPTURE TO THE GROUND STATE THROUGH SUBTHRESHOLD RESONANCES

### A. Contribution of the subthreshold $1^-$ and $2^+$ resonances

While the importance of subthreshold ANCs in the analysis of the  $^{12}\text{C}(\alpha, \gamma)^{16}\text{O}$  reaction was acknowledged and large amount of the literature on this subject has been published (see Ref. [2] and references therein), the precise contribution of the SRs had not been determined previously. From Table V we can already draw some preliminary conclusions about contribution of the pure SRs into the total  $S(300\text{ keV})$  factor. Below we present the calculations of the low-energy  $S$  factors for the  $E1$  and  $E2$  transitions through the subthreshold  $1^-$  and  $2^+$  resonances for capture to the ground state. No other mechanisms are included. It allows us to evaluate numerically

<sup>6</sup>The impact of the interference of the SR with the direct capture will be checked below by using the higher ground-state ANC of  $337\text{ fm}^{-1/2}$ .

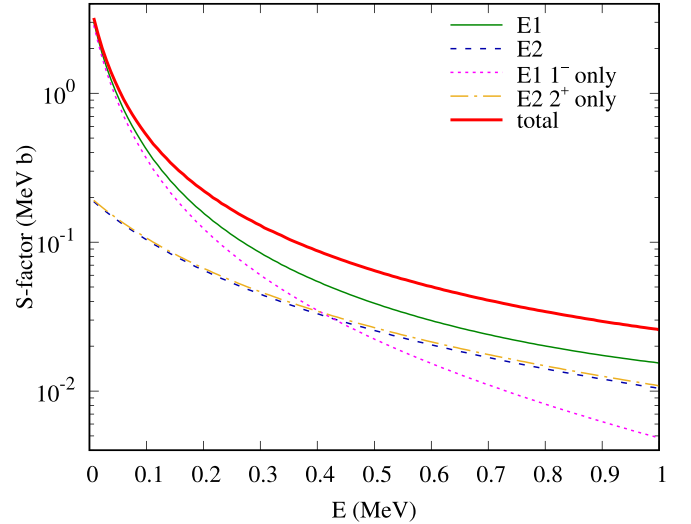


FIG. 5. Low-energy  $S$  factors for the  $^{12}\text{C}(\alpha, \gamma)^{16}\text{O}$  reaction calculated using all the subthreshold and ground-state ANCs from Ref. [2] (see Table I). The thick solid line is the total  $S$  factor, the thin solid line is the total  $E1$   $S$  factor and the dashed line is the total  $E2$   $S$  factor; the dotted line and dot-dashed lines are the  $E1$  and  $E2$   $S$  factors contributed only by the  $1^-$  and  $2^+$  subthreshold resonance transitions to the ground state, respectively. Note that the dashed and dot-dashed lines practically coincide.

the contribution of the SRs to the total low-energy  $S$  factor, and, in particular,  $S(300\text{ keV})$  factors. We then can determine the role of the subthreshold ANCs and show the necessity to decrease their uncertainties to improve the uncertainty of the total  $S(300\text{ keV})$  factor.

Figures 5–7 depict the results of the calculations. In Fig. 5 we use the low ANCs from Ref. [2] (see Table I) including the ground-state ANC  $C_0 = 58\text{ fm}^{-1/2}$ . In Fig. 6 the ground-state ANC remains low (the same as in Fig. 5), while the subthreshold ANCs are higher than in Fig. 5 (the last row of Table I). In Fig. 7 we use higher subthreshold ANCs (as in Fig. 6) and higher ground-state ANC, which is taken from Ref. [18]:  $C_0 = 337\text{ fm}^{-1/2}$ .

One can see that the  $E1$  and  $E2$  subthreshold  $1^-$  and  $2^+$  resonance transitions to the ground state of  $^{16}\text{O}$  give the dominant contribution to the total low-energy  $S$  factor confirming a pivotal role of the subthreshold ANCs in the calculation of the low-energy  $S$  factor.

The  $S$  factors depicted in Figs. 5 and 6 show very similar behavior near the energy of 300 keV: the  $S$  factors  $S_{E1}^{(\text{SR})}(E)$  for the  $E1$  transition to the ground state proceeding through the  $1^-$  SR are slightly lower than the total  $E1$   $S$  factor  $S_{E1}(E)$ . It agrees with our findings about correlation between the ANC of the subthreshold state  $1^-$  and the total  $S_{E1}(E)$  factor presented in Table V. However, according to Figs. 5 and 6, as well as Table VI, it is evident that the value of  $S_{E1}^{(\text{SR})}(300\text{ keV})$  rises as the subthreshold ANC for the  $1^-$  state increases.

The  $S_{E2}^{(\text{SR})}(300\text{ keV})$  factor for the radiative capture through the SR  $2^+$  exceeds the total  $S_{E2}(300\text{ keV})$  factor only by 3%. It means that we observe a small destructive interference of

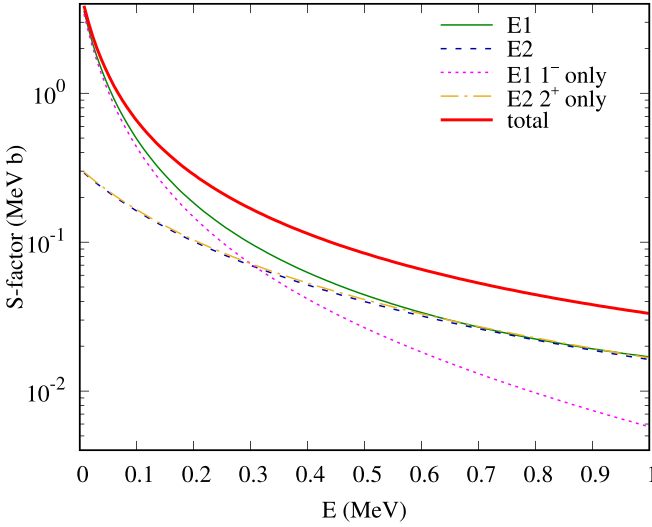


FIG. 6. Low-energy  $S$  factors for the  $^{12}\text{C}(\alpha, \gamma)^{16}\text{O}$  reaction calculated using the ground-state ANC  $C_0(0.0\text{ MeV}) = 58\text{ fm}^{-1/2}$  [2], while all other ANCs are taken from the last two rows of Table I. The notations are the same as in Fig. 5. Note that the dashed and dot-dashed lines practically coincide.

the amplitude for the  $E2$  transition to the ground state through the SR  $2^+$  with the higher broad  $2^+$  resonances and the direct capture amplitudes.

Figure 7 displays the results obtained using the higher subthreshold ANCs (the last two rows in Table I) and the higher ground-state ANC of  $337\text{ fm}^{-1/2}$  [18]. One can see that the behavior of the  $S_{E1}^{(\text{SR})}(E)$  factor is very similar to the one from previous figures proving that this  $S$  factor practically does not depend on the ground-state ANC. The independence of the  $S_{E1}(E)$  factor on the ground-state ANC follows from a simple fact that this dependence can come only from the

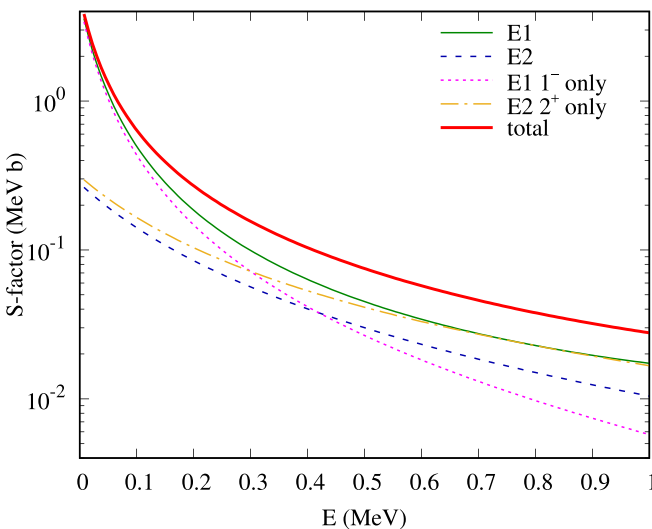


FIG. 7. Low-energy  $S$  factors for the  $^{12}\text{C}(\alpha, \gamma)^{16}\text{O}$  reaction calculated for the ground-state ANC  $C_0(0.0\text{ MeV}) = 337\text{ fm}^{-1/2}$  [18]. All other the ANCs are taken from the last two rows of Table I. The notations are the same as in Fig. 5.

channel radiative transition amplitude  $M_{\text{SR}}^{(\text{ch})}(E)$  of the SR  $1^-$  and direct capture amplitude. However, both contain almost vanishing effective charge, which suppresses the contribution of both amplitudes.

The same is true for the SR  $S_{E2}^{(\text{SR})}(300\text{ keV})$  factor for the  $E2$  transition, which is not sensitive to the ground-state ANC. Still, the total  $S_{E2}(300\text{ keV})$  factor shows a noticeable decrease as the ground-state ANC increases. It means that for the  $E2$  transition we observe the destructive interference of the capture through the SR with the direct transition, which depends on the ground-state ANC. For the small ground-state ANC of  $58\text{ fm}^{-1/2}$  this interference is very small but it becomes significant for the higher ground-state ANC.

The numerical results of the calculations presented in Figs. 5–7 are summarized in Table VI. We see that increase of the subthreshold ANCs increases  $S_{E1}^{(\text{SR})}(300\text{ keV})$  and  $S_{E2}^{(\text{SR})}(300\text{ keV})$ . However, the contribution of the  $S_{E1}^{(\text{SR})}(300\text{ keV})$  (7th column) to the budget of the total  $S_{E1}(300\text{ keV})$  changes very little, 71–74% and does not depend on the ground-state ANC.

The  $S_{E2}^{(\text{SR})}(300\text{ keV})$  also does not depend on the ground-state ANC because the channel radiative width amplitude for the  $E2$  transition is very small. But the total  $S_{E2}(300\text{ keV})$  depends on the ground-state ANC due to the destructive interference of the  $E2$  SR amplitude with the direct capture amplitude to the ground state of  $^{16}\text{O}$ . It results in decrease of the  $S_{E2}(300\text{ keV})$  compared to the  $S_{E2}^{(\text{SR})}(300\text{ keV})$  (eighth column in Table VI).

## B. Impact of the ground-state ANC

Here, we revisit the role of the ground-state ANC once again. In this paper we employed two ground-state ANCs,  $58\text{ fm}^{-1/2}$  [2] and  $337\text{ fm}^{-1/2}$  [18].

As we mentioned above, for the low ground-state ANC the interference of the resonance  $E1$  and  $E2$  transitions with the direct captures to the ground state is small. The present calculations of the  $E1$  and  $E2$  transitions with the ground-state ANC of  $337\text{ fm}^{-1/2}$  and the subthreshold  $1^-$  and  $2^+$  ANCs from Ref. [22] (see also Table I), which include the interference of the resonances and direct captures, resulted in  $S_{E1}(300\text{ keV}) = 99\text{ keVb}$  and  $S_{E2}(300\text{ keV}) = 56\text{ keVb}$ .

Our findings indicate that a notable rise in the ground-state ANC of  $^{16}\text{O}$  has a minimal impact on the astrophysical  $S_{E1}(300\text{ keV})$  factor (compare the last two rows in column  $S_{E1}$  of Table VI). However, it does lead to a 20% reduction of the  $S_{E2}(300\text{ keV})$  compared with the  $S_{E2}(300\text{ keV})$  obtained for the lower ground-state ANC (compare the last two rows in column  $S_{E2}$  of Table VI).

Meanwhile, the uptick in the subthreshold ANCs boosts both  $S_{E1}(300\text{ keV})$  and  $S_{E2}(300\text{ keV})$  values. Therefore, we can infer that the concurrent increase of the subthreshold and ground-state ANCs leads to a boost of the  $S_{E1}(300\text{ keV})$  and  $S_{E2}(300\text{ keV})$  values mitigated by a reduction of the latter at higher ground-state ANC. From Table VI we can see that the total  $S$  factor  $S(300\text{ keV}) = 130\text{ keVb}$  calculated for low subthreshold and the ground-state ANCs elevates to  $168\text{ keVb}$  for higher subthreshold ANCs and low the ground-state ANC,

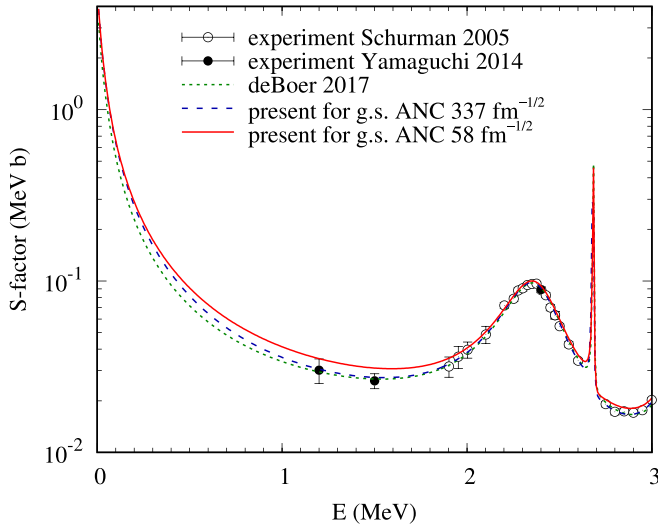


FIG. 8. The total  $S$  factors for the  $^{12}\text{C}(\alpha, \gamma)^{16}\text{O}$  reaction given by  $E1 + E2 +$  cascade transitions to the ground state of  $^{16}\text{O}$  for three different calculations. The solid line is the present total  $S$  factor for the ground-state ANC of  $58 \text{ fm}^{-1/2}$  and the current ANCs of the subthreshold states (the last two rows in Table I); the dashed line is similar to the solid line but for the ground-state ANC of  $337 \text{ fm}^{-1/2}$ ; the dotted line is the total  $S$  factor from deBoer *et al.* [2]. The experimental data are from Schürmann *et al.* [3] and Yamaguchi *et al.* [37].

but it decreases to 155 keVb for the higher subthreshold and ground-state ANCs.

Hence, our calculations confirm a correlation between the ground-state ANC of  $^{16}\text{O}$  and the ANC of the subthreshold  $2^+$  state, in agreement with Ref. [18]. From this perspective, taking into account the results from Ref. [2] and adopting the ANC for the  $2^+$  state from Ref. [22], we can assume that the ground-state ANC of  $^{16}\text{O}$ , which fits the  $S$  factor from Ref. [2], should be less than  $337 \text{ fm}^{-1/2}$ .

Finally, we point out that one of the main uncertainties of the ground-state ANC from Ref. [18], which we use in this paper, stems from the uncertainty of the ANC for  $^{11}\text{B} \rightarrow \alpha + ^7\text{Li}$ , which was not properly discussed in Ref. [18]. That is why at this stage, due to the lack of reliable ANC for the ground state of  $^{16}\text{O}$ , we cannot provide the total uncertainty of the ground-state ANC of  $^{16}\text{O}$  extracted in Ref. [18].

Figure 8 shows the total  $S$  factors contributed by the sum of the  $E1 + E2$  resonance transitions to the ground state of  $^{16}\text{O}$  (including the interference with the direct captures) plus the cascade transition to the ground state of  $^{16}\text{O}$ . There are many experimental datasets available in the literature [2]. We show one of them as a representative example. The explanation of the three different lines is given in the caption to the figure. It is evident that increasing the ground-state ANC and the subthreshold ANCs is bringing the present results closer to those in Ref. [2], which were obtained using lower ANCs.

## VI. SUMMARY

The  $S$  factors for the  $^{12}\text{C}(\alpha, \gamma)^{16}\text{O}$  reaction are calculated within the  $R$ -matrix AZURE2 code using the recently de-

termined ANCs for four subthreshold states  $0_2^+$ ,  $3^-$ ,  $2^+$ ,  $1^-$  [21,22], which represent the high end of the ANCs, and a low ground-state ANC of  $58 \text{ fm}^{-1/2}$  of  $^{16}\text{O}$  [2]. The results are compared with the those obtained in Ref. [2] using the subthreshold ANCs available in the literature, which represents the lower end of the ANCs. Our comprehensive calculations of the low-energy  $S$  factors encompass the  $E1$  and  $E2$  SR transitions to the ground state of  $^{16}\text{O}$ , which interfere with the higher resonances and direct captures, and cascade radiative captures to the ground state of  $^{16}\text{O}$  through four subthreshold states:  $0_2^+$ ,  $3^-$ ,  $2^+$ , and  $1^-$ . Since our ANCs are higher than those used by deBoer *et al.* [2], the present total  $S$  factor at the most effective astrophysical energy of 300 keV is 174 keVb versus 137 keVb of that work. Higher subthreshold bound-state ANCs used in the present calculations lead to a higher  $S(300 \text{ keV})$  factor and higher low-temperature reaction rates (see Appendix B).

Since in the present calculations, all the parameters, except for the subthreshold ANCs, were taken from Ref. [2], we are able to check the dependence of the  $S$  factors for the  $^{12}\text{C}(\alpha, \gamma)^{16}\text{O}$  radiative capture at very low energies, where the resonance captures through the subthreshold state dominate. The contributions of the  $E1$  and  $E2$  SR transitions to the total  $S$  factors  $S_{E1}(300 \text{ keV})$  [ $S_{E2}(300 \text{ keV})$ ] are 71% and 74% (102% and 103%) for the subthreshold ANCs from Ref. [2] and present ones, respectively. Moreover, we also observe that for the uncertainty of the  $1^-$  ( $2^+$ ) subthreshold ANC of 19% (55%) generates 15% (56%) uncertainty in the  $S_{E1}(300 \text{ keV})$  [ $S_{E2}(300 \text{ keV})$ ]. It is essential to emphasize that the ratio  $S_{E1}^{(\text{SR})}(300 \text{ keV})/S_{E1}(300 \text{ keV}) = 74\%$  is less than the correlation of the uncertainties  $\Delta C_1^2$  and  $\Delta S_{E1}(300 \text{ keV})$ , which is 79%. This arises from the additional contribution of the interference of the  $E1$  SR and the broad (9.59 MeV,  $1^-$ ) resonance, which also depends on  $C_1$ .

The  $E1$  transition of the SR  $1^-$  is not influenced by the ground-state ANC as the  $E1$  nonresonant capture is the isospin forbidden transition (with a negligibly small effective charge), yet it still interferes constructively with a broad (9.585 MeV;  $1^-$ ) resonance giving (for the present subthreshold ANCs) an additional 26% contribution to the total  $S_{E1}(300 \text{ keV})$  factor.

The interference between the  $E2$  transition of the SR  $2^+$  and direct capture is minimal when the ground-state ANC is small, but becomes destructive at higher ground-state ANC, resulting in a contribution of  $-29\%$ . The low-energy  $S_{E2}(300 \text{ keV})$  factor experiences a smaller increase when both subthreshold and the ground-state ANCs rise together due to their anticorrelation, compared to when only the subthreshold ANCs increase.

In summary, our key findings indicate that:

(1) For given parameters of the broad  $1^-$  resonance 9.59 MeV [2] we can control the uncertainty of the  $S_{E1}(300 \text{ keV})$  factor, which stems from the uncertainty of the square of the subthreshold ANC  $C_1^2$ , as the total uncertainty of the former is 79% of the latter.

(2) The uncertainty in the ground-state ANC limits the conclusiveness of our analysis for the  $E2$  transition compared to the  $E1$  case. The most pressing issue that needs attention is determining the ground-state ANC.

Nevertheless, we can draw some preliminary conclusions. For the low ground-state ANC, the uncertainty of the  $S_{E2}(300\text{ keV})$  factor is completely generated by the uncertainty of  $C_2^2$ . Hence, the total uncertainty of the  $S(300\text{ keV})$  factor is given by  $\sqrt{[0.79 \Delta C_1^2]^2 + [\Delta C_2^2]^2}$ . An increase in the ground-state ANC results in a decrease in the contribution of the  $S_{E2}(300\text{ keV})$  to the total  $S(300\text{ keV})$  factor, making the uncertainty in  $C_2^2$  less important. Therefore, we can assert that the upper bound of the total uncertainty for the  $S(300\text{ keV})$  is  $\sqrt{[0.79 \Delta C_1^2]^2 + [\Delta C_2^2]^2}$ .

### ACKNOWLEDGMENTS

R.J.D. utilized resources from the Notre Dame Center for Research Computing and was supported by the National Science Foundation through Grants No. PHY-1713857 and No. PHY-2011890, and the Joint Institute for Nuclear Astrophysics through Grant No. PHY-1430152 (JINA Center for the Evolution of the Elements). A.S.K. acknowledges the support from the Australian Research Council.

### APPENDIX A: REDUCED WIDTH OF THE SUBTHRESHOLD RESONANCE

Discussing the appearance of the Whittaker function in Eq. (18) is appropriate and ties in with deriving the expression for the reduced width of the SR. To establish a relationship between  $\Gamma_{J_s}^{\text{SR}}(E)$ ,  $\gamma_{l_s}^{\text{SR}}(R_{\text{ch}})$  and the ANC  $C_{l_s}$  of the subthreshold bound state, one can extrapolate the elastic scattering  $S$  matrix [see Eq. (3)] to the SR pole.

The fundamental concept of the  $S$  matrix's analyticity requires the existence of a bound-state pole positioned on the upper part of the imaginary axis in the  $k$  plane. In the vicinity of the subthreshold pole in the  $k$  plane, the  $S$  matrix for elastic scattering is represented by [25]

$$S_{l_s} \stackrel{k \rightarrow i\kappa_s + 0}{=} -i(-1)^{l_s} e^{i\pi\eta_s} \frac{C_{l_s}^2}{k - i\kappa_s}. \quad (\text{A1})$$

In this equation, the pole's residue is articulated in terms of the subthreshold ANC  $C_{l_s}$ .

At the same time, the elastic scattering  $S$  matrix in the  $R$ -matrix approach can be written in terms of the resonance width or, alternatively, in terms of the reduced width. To make the derivation of the  $S$  matrix in the presence of the SR clearer, we start from the beginning. In the  $R$ -matrix formalism, the single-level, single-channel  $S$  matrix is provided by

$$S_{l_s} = e^{-2i(\delta_{c_{l_s}}^{\text{hs}} - \sigma_{c_{l_s}}^c)} \frac{1/R_{l_s} - [\Delta_{l_s}(E) - B_{l_s} - iP_{l_s}(k, R_{\text{ch}})]}{1/R_{l_s} - [\Delta_{l_s}(E) - B_{l_s} + iP_{l_s}(k, R_{\text{ch}})]}, \quad (\text{A2})$$

where  $R_{l_s} = \tilde{\gamma}_{l_s}^2/(E_s - E)$  is the  $R$  matrix,  $\tilde{\gamma}_{l_s}^2$  is the formal reduced width of the subthreshold level. Additionally,  $\Delta_{l_s}(E)$  is the Thomas shift and  $B_{l_s}$  is the boundary condition. We remind that  $J_s = l_s$ .  $E_s$  is the  $R$ -matrix-level energy corresponding to the subthreshold resonance. We adopt  $E_s = -\varepsilon_s$

and  $B_{l_s} = \Delta_{l_s}(-\varepsilon_s)$ . Then for  $E$  in the vicinity of  $-\varepsilon_s$

$$S_{l_s} \approx e^{-2i(\delta_{c_{l_s}}^{\text{hs}} - \sigma_{c_{l_s}}^c)} \frac{-\varepsilon_s - E + iP_{l_s}(k, R_{\text{ch}}) \gamma_{l_s}^2}{-\varepsilon_s - E - iP_{l_s}(k, R_{\text{ch}}) \gamma_{l_s}^2}. \quad (\text{A3})$$

We employed  $\Delta_{l_s}(E) - \Delta_{l_s}(-\varepsilon_s) \approx \frac{d\Delta_{l_s}(E)}{dE}|_{E=-\varepsilon_s} (E + \varepsilon_s)$ . It allows one to introduce the observable reduced width:

$$[\gamma_{l_s}^{\text{SR}}(R_{\text{ch}})]^2 = \frac{\tilde{\gamma}_{l_s}^2}{1 + \frac{d\Delta_{l_s}(E)}{dE}|_{E=-\varepsilon_s}}. \quad (\text{A4})$$

When extrapolating  $E \rightarrow -\varepsilon_s$  Eq. (A3) is reduced to

$$S_{l_s} \stackrel{E \rightarrow -\varepsilon_s}{\approx} -i e^{-2i(\delta_{c_{l_s}}^{\text{hs}} - \sigma_{c_{l_s}}^c)} \frac{P_{l_s}(k, R_{\text{ch}}) [\gamma_{l_s}^{\text{SR}}(R_{\text{ch}})]^2}{E + \varepsilon_s}. \quad (\text{A5})$$

To obtain it we took into account that in the denominator at  $E \leq 0$   $\Gamma_{J_s}^{\text{SR}}(E) = 0$  due to the presence in it the barrier penetrability  $P_l(k, R_{\text{ch}})$  [see Eq. (13)], which represents the imaginary component of the logarithmic derivative of the wave function that remains real for negative energies. However, taking into account Eq. (12), the numerator is made up of

$$\begin{aligned} e^{2i(\sigma_{l_s}^c - \delta_{l_s}^{\text{hs}})} P_{l_s}(k, R_{\text{ch}}) &= \frac{k R_{\text{ch}}}{[O_{l_s}(k, R_{\text{ch}})]^2} \\ &= \frac{(-1)^{l_s} e^{-\pi\eta \text{sign Re}k} k R_{\text{ch}}}{[W_{-i\eta, l_s+1/2}(-2ik R_{\text{ch}})]^2}. \end{aligned} \quad (\text{A6})$$

TABLE VII. Low-temperature reaction rates ( $T_9 \leq 2$ ).

$T_9$	Reaction Rates ( $\frac{\text{cm}^3}{\text{s mol}}$ )	
	Present	Ref. [2]
0.06	$6.81 \times 10^{-26}$	$6.78 \times 10^{-26}$
0.07	$3.65 \times 10^{-24}$	$3.28 \times 10^{-24}$
0.08	$9.33 \times 10^{-23}$	$8.00 \times 10^{-23}$
0.09	$1.42 \times 10^{-21}$	$1.18 \times 10^{-21}$
0.1	$1.46 \times 10^{-20}$	$1.20 \times 10^{-21}$
0.11	$1.11 \times 10^{-19}$	$9.03 \times 10^{-20}$
0.12	$6.66 \times 10^{-19}$	$5.38 \times 10^{-19}$
0.13	$3.29 \times 10^{-18}$	$2.65 \times 10^{-18}$
0.14	$1.39 \times 10^{-17}$	$1.11 \times 10^{-17}$
0.15	$5.11 \times 10^{-17}$	$4.08 \times 10^{-17}$
0.16	$1.68 \times 10^{-16}$	$1.34 \times 10^{-16}$
0.18	$1.37 \times 10^{-15}$	$1.09 \times 10^{-16}$
0.20	$8.34 \times 10^{-15}$	$6.64 \times 10^{-15}$
0.30	$4.68 \times 10^{-12}$	$3.73 \times 10^{-12}$
0.35	$4.10 \times 10^{-11}$	$3.28 \times 10^{-11}$
0.4	$2.44 \times 10^{-10}$	$1.96 \times 10^{-10}$
0.45	$1.10 \times 10^{-9}$	$8.82 \times 10^{-10}$
0.5	$3.99 \times 10^{-9}$	$3.22 \times 10^{-9}$
0.6	$3.33 \times 10^{-8}$	$2.70 \times 10^{-8}$
0.7	$1.80 \times 10^{-7}$	$1.47 \times 10^{-7}$
0.8	$7.2 \times 10^{-7}$	$5.92 \times 10^{-7}$
0.9	$2.32 \times 10^{-6}$	$1.92 \times 10^{-6}$
1.0	$6.37 \times 10^{-6}$	$5.30 \times 10^{-6}$
1.25	$4.85 \times 10^{-5}$	$4.10 \times 10^{-6}$
2.0	$2.60 \times 10^{-3}$	$2.40 \times 10^{-3}$

$e^{\pi \eta \text{sign Re}k} [W_{-i\eta, l_s+1/2}(k, R_{\text{ch}})]^2$  is analytic function in the upper half  $k$  plane ( $\text{Im}k > 0$ ) except the point  $k = 0$  [25]. Its extrapolation to the subthreshold bound state pole is simple, leading to the emergence of the Whittaker function  $W_{-\eta_s, l_s+1/2}(2\kappa_s R_{\text{ch}})$  for the subthreshold bound state:

$$e^{2i(\sigma_{l_s}^c - \delta_{l_s}^{\text{hs}})} P_{l_s}(k, R_{\text{ch}}) \stackrel{k \rightarrow i\kappa_s}{=} \frac{(-1)^{l_s} e^{i\pi \eta_s} i \kappa_s R_{\text{ch}}}{[W_{-\eta_s, l_s+1/2}(2\kappa_s R_{\text{ch}})]^2}. \quad (\text{A7})$$

With Eq. (A7) considered, in the vicinity of the subthreshold bound state pole in the  $k$  plane Eq. (A5) transforms to

$$S_{l_s} \stackrel{k \rightarrow i\kappa_s}{\approx} -i \mu R_{\text{ch}} \frac{(-1)^{l_s} e^{i\pi \eta_s} [\gamma_{l_s}^{\text{SR}}(R_{\text{ch}})]^2}{[W_{-\eta_s, l_s+1/2}]^2} \frac{1}{k - i\kappa_s}. \quad (\text{A8})$$

Equation (18) is derived from the comparison of Eqs. (A1) and (A8).

## APPENDIX B: REACTION RATES

In Table VII we compare the reaction rates calculated using the present total  $S$  factor with the ones from Ref. [2]. For easier comparison, the tabulated low-temperature reaction rates are calculated at the same temperatures as in Ref. [2]. Since the present  $S$  factor is larger than that from Ref. [2], at low temperatures  $T_9 < 2.0$  our reaction rates exceed the reaction rates from Ref. [2]. However, since we constrain our calculations to low-energy  $S$  factor, at temperatures  $T_9 \geq 2$  the reaction rates from Ref. [2] exceed ours.

- 
- [1] C. E. Rolfs and W. S. Sydney, *Cauldrons in the Cosmos* (University of Chicago Press, Chicago, IL, 1988).
- [2] R. J. de Boer, J. Görres, and M. Wiescher, R. E. Azuma, A. Best, C. R. Brune, C. E. Fields, S. Jones, M. Pignatari, D. Sayre, K. Smith, and F. X. Timmes, *Rev. Mod. Phys.* **89**, 035007 (2017).
- [3] D. Schürmann, A. Di Leva *et al.*, *Eur. Phys. J. A* **26**, 301 (2005).
- [4] A. Redder, H. W. Becker, C. Rolfs, H. P. Trautwetter, T. R. Donoghue, T. C. Rinckel, J. W. Hammer, and K. Langanke, *Nucl. Phys. A* **462**, 385 (1987).
- [5] R. M. Kremer, C. A. Barnes, K. H. Chang, H. C. Evans, B. W. Filippone, K. H. Hahn, and L. W. Mitchell, *Phys. Rev. Lett.* **60**, 1475 (1988).
- [6] F. C. Barker and T. Kajino, *Aust. J. Phys.* **44**, 369 (1991).
- [7] J. M. L. Ouellet, H. C. Evans, H. W. Lee, J. R. Leslie, J. D. MacArthur, W. McLatchie, H.-B. Mak, P. Skensved, J. L. Whitton, X. Zhao, and T. K. Alexander, *Phys. Rev. Lett.* **69**, 1896 (1992).
- [8] R. E. Azuma, L. Buchmann, F. C. Barker, C. A. Barnes, J. M. D'Auria, M. Dombisky, U. Giesen, K. P. Jackson, J. D. King, R. G. Korteling, P. McNeely, J. Powell, G. Roy, J. Vincent, T. R. Wang, S. S. M. Wong, and P. R. Wrean, *Phys. Rev. C* **50**, 1194 (1994).
- [9] C. R. Brune, W. H. Geist, R. W. Kavanagh, and K. D. Veal, *Phys. Rev. Lett.* **83**, 4025 (1999).
- [10] R. Kunz, M. Jaeger, A. Mayer, J. W. Hammer, G. Staudt, S. Harissopulos, and T. Paradellis, *Phys. Rev. Lett.* **86**, 3244 (2001).
- [11] M. Assunção, M. Fey, A. Lefebvre-Schuhl, J. Kiener, V. Tatischeff, J. W. Hammer, C. Beck, C. Boukari-Pelissie, A. Coc, J. J. Correia, S. Courtin, F. Fleurot, E. Galanopoulos, C. Grama, F. Haas, F. Hammache, F. Hannach, S. Harissopulos, A. Korichi, R. Kunz *et al.*, *Phys. Rev. C* **73**, 055801 (2006).
- [12] A. Belhout, S. Ouichaoui, H. Beaumevielle, A. Boughrara, S. Fortier, J. Kiener, J. M. Maison, S. K. Mehdi, L. Rosier, J. P. Thibaud, A. Trabelsi, and J. Vernotte, *Nucl. Phys. A* **793**, 178 (2007).
- [13] R. Plag, R. Reifarth, M. Heil, F. Käppeler, G. Rupp, F. Voss, and K. Wisshak, *Phys. Rev. C* **86**, 015805 (2012).
- [14] D. B. Sayre, C. R. Brune, D. E. Carter, D. K. Jacobs, T. N. Massey, and J. E. O'Donnell, *Phys. Rev. Lett.* **109**, 142501 (2012).
- [15] D. Schürmann, L. Gialanella, R. Kunz, and F. Strieder, *Phys. Lett. B* **711**, 35 (2012).
- [16] M. Gai, *Phys. Rev. C* **88**, 062801(R) (2013).
- [17] M. L. Avila, G. V. Rogachev, E. Koshchiy, L. T. Baby, J. Belarge, K. W. Kemper, A. N. Kuchera, A. M. Mukhamedzhanov, D. Santiago-Gonzalez, and E. Uberseder, *Phys. Rev. Lett.* **114**, 071101 (2015).
- [18] Y. Shen, B. Guo, R. J. de Boer, E. Li, Zh. Li, Y. Li, X. Tang, D. Pang, S. Adhikari, Ch. Basu, J. Su, Sh. Yan, Q. Fan, J. Liu, Ch. Chen, Zh. Han, X. Li, G. Lian, T. Ma, W. Nan *et al.*, *Astrophys. J.* **945**, 41 (2023).
- [19] L. D. Blokhintsev, A. S. Kadyrov, A. M. Mukhamedzhanov, and D. A. Savin, *Phys. Rev. C* **95**, 044618 (2017).
- [20] L. D. Blokhintsev, A. S. Kadyrov, A. M. Mukhamedzhanov, and D. A. Savin, *Phys. Rev. C* **97**, 024602 (2018).
- [21] L. D. Blokhintsev, A. S. Kadyrov, A. M. Mukhamedzhanov, and D. A. Savin, *Eur. Phys. J. A* **58**, 257 (2022).
- [22] L. D. Blokhintsev, A. S. Kadyrov, A. M. Mukhamedzhanov, and D. A. Savin, *Eur. Phys. J. A* **59**, 162 (2023).
- [23] S. B. Dubovichenko, A. S. Tkachenko, R. Ya. Kezerashvili, N. A. Burkova, and A. V. Dzhezairov-Kakhramanov, *Phys. Rev. C* **105**, 065806 (2022); E. M. Tursunov, S. A. Turakulov, and K. I. Tursunmakhatov, *ibid.* **108**, 065801 (2023).
- [24] A. M. Mukhamedzhanov, *Eur. Phys. J. A* **59**, 43 (2023).
- [25] A. M. Mukhamedzhanov and L. D. Blokhintsev, *Eur. Phys. J. A* **58**, 29 (2022).
- [26] A. M. Mukhamedzhanov and R. E. Tribble, *Phys. Rev. C* **59**, 3418 (1999).
- [27] N. Oulevsir, F. Hammache, P. Roussel, M. G. Pellegriti, L. Audouin, D. Beaumel, A. Bouda, P. Descouvemont, S. Fortier, L. Gaudefroy, J. Kiener, A. Lefebvre-Schuhl, and V. Tatischeff, *Phys. Rev. C* **85**, 035804 (2012).
- [28] Yu. V. Orlov, B. F. Irgaziev, and L. I. Nikitina, *Phys. Rev. C* **93**, 014612 (2016).
- [29] Yu. V. Orlov, B. F. Irgaziev, and Jameel-Un Nabi, *Phys. Rev. C* **96**, 025809 (2017).
- [30] O. L. Ramírez Suárez and J.-M. Sparenberg, *Phys. Rev. C* **96**, 034601 (2017).
- [31] Shung-Ichi Ando, *Phys. Rev. C* **97**, 014604 (2018).
- [32] Yu. V. Orlov, *Nucl. Phys. A* **1014**, 122257 (2021); **1018**, 122385(E) (2022).
- [33] C. Hebborn, M. L. Avila, K. Kravvaris, G. Potel, and S. Quaglioni, *Phys. Rev. C* **109**, L061601 (2024).
- [34] D. R. Tilley, H. R. Weller, and C. M. Cheves, *Nucl. Phys. A* **564**, 1 (1993).

- [35] J. M. Eisenberg and W. Greiner, *Excitation Mechanisms of the Nucleus: Electromagnetic and Weak Interactions* (North-Holland Publishing Company, Amsterdam, 1970).
- [36] D. Baye and E. Tursunov, [J. Phys. G \*\*45\*\*, 085102 \(2018\)](#),
- [37] H. Yamaguchi, K. Sagara, K. Fujita, D. Kodama, Y. Narikiyo, K. Hamamoto, T. Ban, N. Tao, and T. Teranishi, [AIP Conf. Proc. \*\*1594\*\*, 229 \(2014\)](#).